AD-A126 349 DYNAMIC ICE-STRUCTURE INTERACTION DURING CONTINUOUS CRUSHING(U) COLD REGIONS RESEARCH AND ENGINEERING LAB HANOVER NH M MAATTANEN FEB 83 CRREL-83-5 1/1

UNCLASSIFIED F/G 8/12 NL

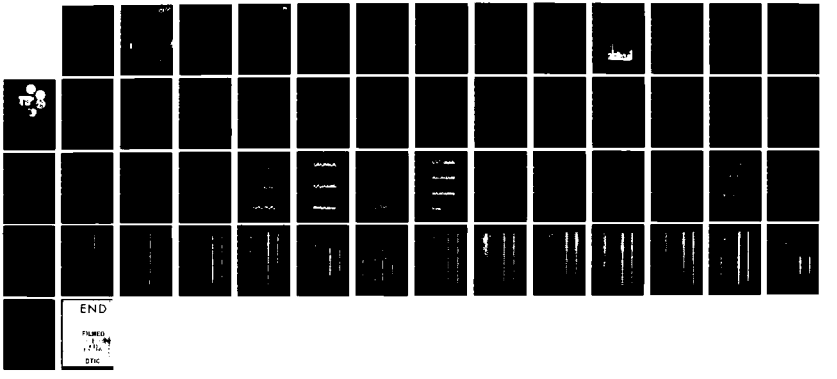

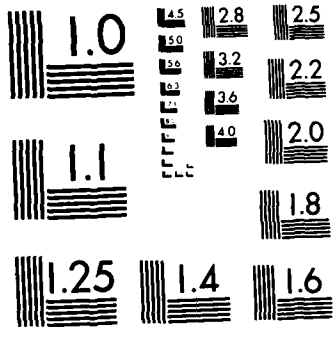

MICROCOPY RESOLUTION TEST CHART
NATIONAL BUREAU OF STANDARDS 1963-A

CRREL
REPORT 83-5

US Army Corps of Engineers
Cold Regions Research & Engineering Laboratory

Dynamic ice-structure interaction during continuous crushing

For conversion of SI metric units to U.S./ British customary units of measurement consult ASTM Standard E380, Metric Practice Guide, *published by the American Society for Testing and Materials, 1916 Race St., Philadelphia, Pa. 19103.*

Cover: Dynamic ice-structure interaction in the field similar to the case simulated in the laboratory and analyzed in this report.

CRREL Report 83-5

February 1983

Dynamic ice-structure interaction during continuous crushing

Mauri Määttänen

Prepared for
U.S. ARMY EUROPEAN RESEARCH OFFICE
Approved for public release; distribution unlimited

Unclassified

SECURITY CLASSIFICATION OF THIS PAGE *(When Data Entered)*

REPORT DOCUMENTATION PAGE		READ INSTRUCTIONS BEFORE COMPLETING FORM
1. REPORT NUMBER CRREL Report 83-5	2. GOVT ACCESSION NO. AD-A126 349	3. RECIPIENT'S CATALOG NUMBER
4. TITLE *(and Subtitle)* DYNAMIC ICE-STRUCTURE INTERACTION DURING CONTINUOUS CRUSHING		5. TYPE OF REPORT & PERIOD COVERED 6. PERFORMING ORG. REPORT NUMBER
7. AUTHOR(s) Mauri Määttänen		8. CONTRACT OR GRANT NUMBER(s)
9. PERFORMING ORGANIZATION NAME AND ADDRESS U.S. Army Cold Regions Research and Engineering Laboratory Hanover, New Hampshire 03755		10. PROGRAM ELEMENT, PROJECT, TASK AREA & WORK UNIT NUMBERS DAJA37-79-RO474
11. CONTROLLING OFFICE NAME AND ADDRESS U.S. Army European Research Office London, England		12. REPORT DATE February 1983 13. NUMBER OF PAGES 53
14. MONITORING AGENCY NAME & ADDRESS*(if different from Controlling Office)*		15. SECURITY CLASS. *(of this report)* Unclassified 15a. DECLASSIFICATION/DOWNGRADING SCHEDULE

16. DISTRIBUTION STATEMENT *(of this Report)*

Approved for public release; distribution unlimited.

17. DISTRIBUTION STATEMENT *(of the abstract entered in Block 20, if different from Report)*

18. SUPPLEMENTARY NOTES

19. KEY WORDS *(Continue on reverse side if necessary and identify by block number)*

Ice
Structural properties
Pile structures

20. ABSTRACT *(Continue on reverse side if necessary and identify by block number)*

This report presents the results of dynamic ice-structure interaction model tests conducted at the CRREL Ice Engineering Facility. A flexible, single-pile, bottom-founded offshore structure was simulated by a test pile with about a one-to-ten scale ratio. Urea (instead of sodium chloride) was used as dopant to scale down the ice properties, resulting in good model ice properties. Six ice fields were frozen and 18 tests carried out. In all cases distinctive dynamic ice-structure interaction vibrations appeared, from which abundant data were collected. In tests with linear ice velocity sweep, sawtooth-shaped ice force fluctuations occurred first. With increasing velocity the natural modes of the test pile were excited, and shifts from one mode to another occurred. The maximum ice force values appeared mostly with low loading rates, but high forces appeared random'y at high ice velocities. As a general trend, ice force

DD FORM 1 JAN 73 1473 EDITION OF 1 NOV 65 IS OBSOLETE

Unclassified

SECURITY CLASSIFICATION OF THIS PAGE *(When Data Entered)*

20. Abstract (cont'd).

maximums, averages and standard deviations decreased with increasing ice velocities. The aspect ratio effect of the ice force in continuous crushing follows the same dependence as in static loadings. The frequency of observed ice forces is strongly dominated by the natural modes of the structure. Dynamically unstable natural modes tend to make the developing ice force frequencies the same as the natural frequencies. Otherwise the resulting frequency depends directly on structural stiffness and ice velocity and inversely on the ice force range. During vibrations the displacement rates of the structure overcome the velocity of ice, making low loading rates and hence high ice forces possible. During crushing, ice induces both positive and negative damping. The latter easily becomes so high that the pile becomes dynamically unstable and is the origin for ice-induced vibrations. As the negative damping effect prevails only during a part of a vibration cycle, the overall state is stable and steady state limit cycles develop. These measured results verify earlier theoretical predictions and confirm a basis for safer design against dynamic ice forces.

PREFACE

This report was prepared by Dr. Mauri Määttänen, Professor of Technical Mechanics, University of Oulu, Finland. The research was carried out at the U.S. Army Cold Regions Research and Engineering Laboratory Ice Engineering Facility in Hanover, New Hampshire. The author is grateful to the U.S. Army European Research Office for funding this research under project DAJA37-79-RO474, which is a continuation of the previous European Research Office project DAERO-78-G-09. He also thanks the University of Oulu for granting him sabbatical to conduct this research. Most of all he is grateful to the CRREL Ice Engineering Facility personnel for their outstanding cooperation in running tests and for their warm and encouraging attitude.

CONTENTS

ILLUSTRATIONS

TABLES

DYNAMIC ICE-STRUCTURE INTERACTION DURING CONTINUOUS CRUSHING

Mauri Määttänen

INTRODUCTION

The interactions between the ice and the structure when a constant-thickness ice sheet crushes against a vertical pile have long been studied, both in the laboratory and in the field. However, due to the limits of the test arrangements, the great number of parameters to be considered, and the complexity of the problem, dynamic ice-structure interactions still are not fully understood.

Most of the research in this field[1-10] has focused on the maximum ice force; dynamic variations have received little or no attention. Most researchers try to avoid dynamic ice-structure interactions by making the loading apparatus as stiff as possible. In addition the stroke of the load actuator has often been so short that continuous crushing interaction is impossible. Only one experiment[11] has tested dynamic ice-structure interactions.

In laboratory tests it is easy to control and vary parameters and to repeat the test if necessary. The difficulty in laboratory tests is scaling the properties of both the ice and the structure correctly. It is not possible to scale down all ice properties simultaneously.[11] The effects of scaling on the relationship between ice strength and loading rate are unknown.

Field tests give valuable data on real ice-structure interaction without any scale effects. The interpretation of the results, however, is more difficult. Usually it is not possible to measure the basic parameters of ice (velocity, thickness, temperature, and grain size and orientation) while the ice is moving. Published reports[5,8,12-14] only give estimates of these parameters. The chances of changing one parameter in the field are minimal.

There are different opinions about the participation of the structure itself in the interaction: most of the authors[7,13,14,16] explained that the dynamic ice force results from the properties of ice alone, while Määttänen[15] proposed that the dynamic response of the structure affects the resulting ice force and ice failure process, so that the properties of both the ice and the structures are significant. With very stiff structures the effect of structural response becomes insignificant, but with slender pile and pier structures the dynamic stiffness plays an important role in the resulting interacting ice force. Earlier tests lacked the power of modern signal-analyzing techniques and the versatility of computer modeling. Now the dynamic properties of the structures related to primary structural parameters (the width and shape of the area exposed to ice actions) can also be assessed.

There have been only two theoretical approaches to the ice-structure interaction problem. Reddy et al.[17] used a statistical approach in which the ice force excitation (assumed to be random) was modified by the properties of the structure to give the dynamic response spectra. In this forced vibration approach no real ice-structure interaction occurs. Määttänen[15] related the ice strength dependence on the loading rate to the deformation rate of the structure at the ice action point. Hence, the ice and the structure form a closed loop system: each affects the other. With this interaction model it is possible to solve the resulting ice force vs time function without any arbitrary assumptions, because only known physical properties of the ice and the structure are used. The least known parameter is the dependence of the ice strength on the loading rate. There exist

only a few measurements of this dependence?[7,10,14] Ice strength is a statistical quantity, and hence the published curves of crushing strength vs loading rate are averages.

This research is a continuation of the dynamic ice-structure interaction tests that started in 1978 at the CRREL Ice Engineering Facility. In its present form the laboratory arrangements allow a number of parameters to be measured: ice and structural properties in a scale from 1:4 to 1:40, temperature ranges from 0° to -20°C, and ice velocities that yield loading rates for ice failure from ductile to brittle. The first report[11] describes dynamic ice-structure interaction test arrangements and procedures, instrumentation, modeling laws and analysis methods. Test results at high velocity range were given. At the most interesting low-velocity range (the transition from ductile to brittle ice failure mode), results were unreliable due to jerking ice movement, which was caused by an ice-pulling mechanism that was too flexible.

The main objective of this research was to measure the dependence of ice forces and crushing frequency on the properties of both the ice and the structure during continuous crushing at the low velocity range. The varied parameters include: ice thickness, pile diameter at the waterline, pile natural frequencies and natural modes. The ice-induced positive and negative damping effects and the stability and limit cycles of self-excited vibrations were also emphasized in the data analysis.

TEST ARRANGEMENTS

The simulation of moving ice crushing against a bottom-founded pile was arranged in the CRREL Ice Engineering Facility so that the scale model of the structure was fixed to the bottom of the test basin and the ice was pushed by a carriage bridge. The velocity of the ice was controlled by a closed loop control system. The normal procedure was to maintain a constant acceleration in order to sweep the whole velocity range in one run.

The actual structures could be scaled with an exact geometrical similitude. Then, however, the structural properties would be difficult to change in subsequent tests. For studying ice-structure interactions it is enough to scale down correctly only those natural modes that contribute significantly to deformations at the ice action point. Therefore, a test pile and supporting structure (Figs. 1 and 2) was designed so that the stiffness, natural frequencies and modes could be easily varied. The width at the waterline and the shape of the area affected by the ice could be varied by changing the collar at the waterline. By this method most of the single-pile, bottom-founded structures could be simulated.

The different configurations of the test pile were calibrated before testing. The transfer function measurement gives all the information about the dynamic properties of the structure. This calibration was carried out by impacting the pile at the waterline with a load cell. From the ratio between the

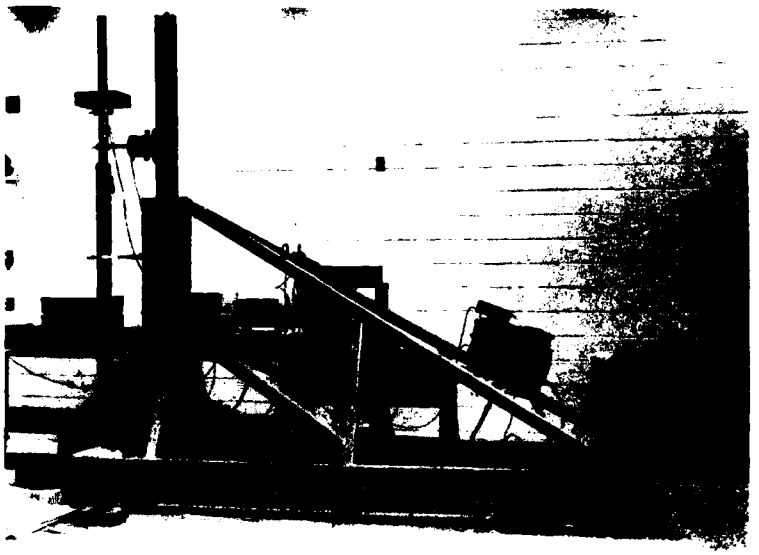

Figure 1. Test pile and supporting structure.

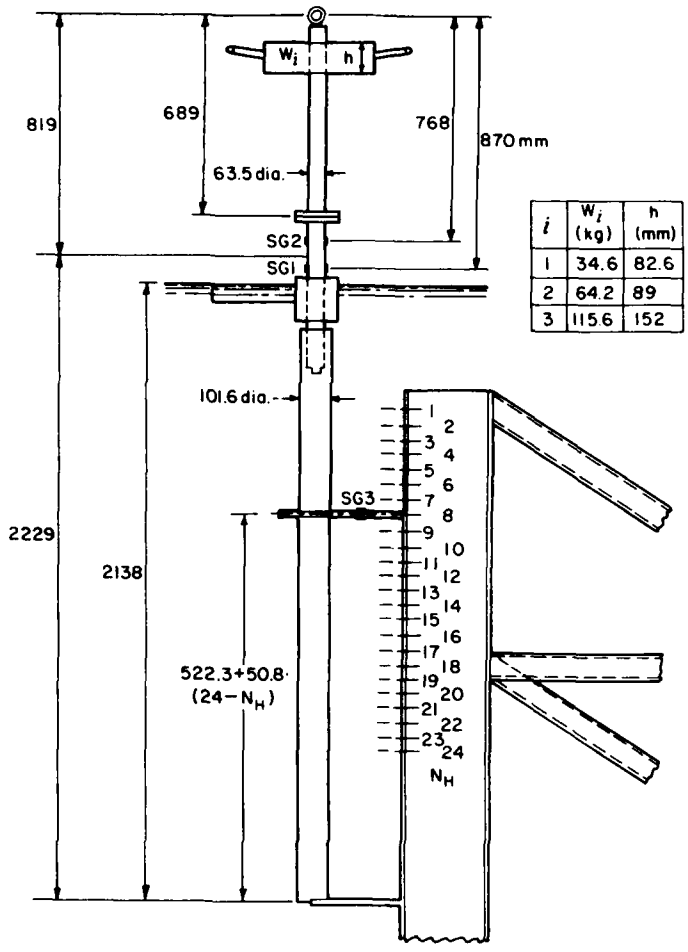

i	W_i (kg)	h (mm)
1	34.6	82.6
2	64.2	89
3	115.6	152

Figure 2. Test pile blueprint.

output signal at the strain gauges in the test pile and the input impact load signal, the transfer function was calculated. Natural frequencies and modal damping are then readily available, and the static stiffness against the ice force can be calculated. Figure 3 shows the transfer and coherence functions for Tests 34-51. In addition, damping was measured from the decay rates of the acceleration signals after impacts. The ranges of the available first and second natural frequencies without and with a superstructure tuning weight are given in Figure 4. Also, the curve for static stiffness is presented as a function of test pile support location.

The instrumentation in the test pile included strain gauges used to measure the reaction of the ice force at the upper support clamp. In the superstructure just above the waterline were two sets of strain gauges used to measure the bending moment and shear force, both of which were used to eliminate the inertial effects of the superstructure on the ice force. Accelerometers on the superstructures could be attached at different levels and in different directions; they were used to measure the dynamic response. In some tests one accelerometer was installed on the ice or on the carriage for measuring ice jerking. The instruments for recording and analyzing data and the analyzing procedures are the same as explained by Määttänen.[11] Figure 5 shows the signal recording and processing block diagram.

As an improvement to the first test setup,[11] the test carriage bridge was used to pull the ice in the test basin. However, neither of its test setups was capable of providing velocities low enough for ice-structure interaction tests. Therefore, the main drive of the test carriage was disconnected and its reduction gear removed; they were replaced by the DC-drive and reduction gear from the previous test setup.[11] Then the reduction gear was driving the drive shafts of the carriage instead of winches. This gave a controllable speed range from 4 to 104 mm/s. With the scaling factors the loading rate corresponding to the transition in ice strength from ductile to brittle was about 10 mm/s. The average stress rate that could be achieved ranged from 80 to 6000 kPa/s.

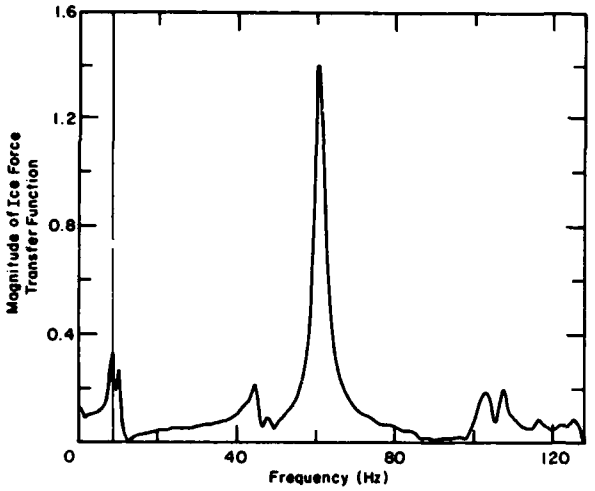

a. Transfer function ice force to support reaction in the clamp (tests 37–42 and 45–51).

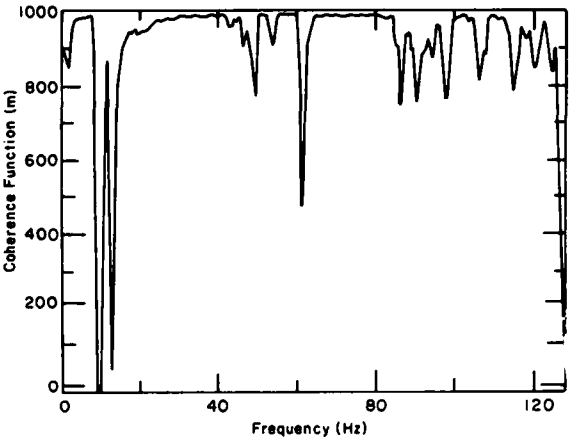

b. Coherence function ice force to support reaction in the clamp (tests 37–42 and 45–51).

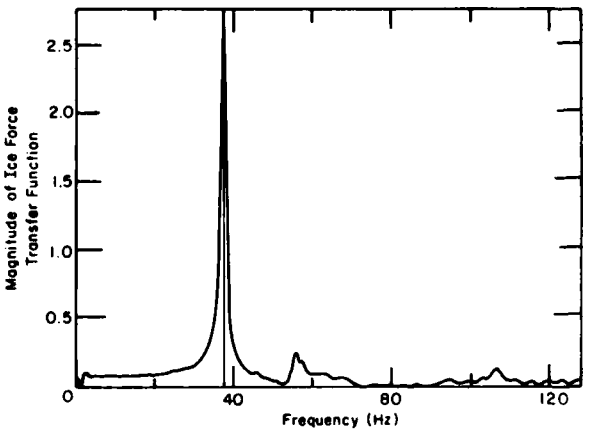

c. Transfer function ice force to support reaction in the clamp (tests 43–44).

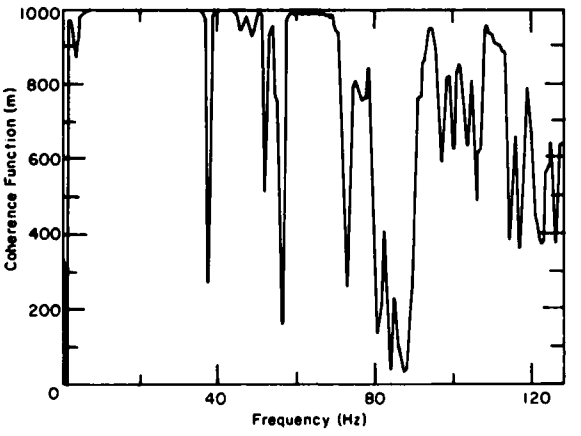

d. Coherence function ice force to support reaction in the clamp (tests 43–44).

Figure 3. Transfer and coherence functions.

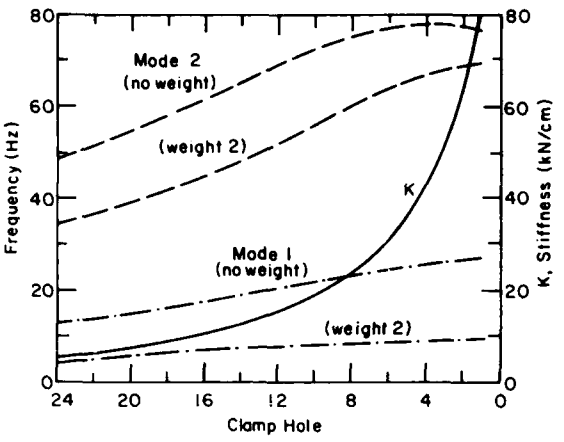

Figure 4. Test pile natural frequencies and stiffness vs support clamp attachment position.

The only shortcoming of the test arrangements was the stiffness of the ice-pulling system, despite the improvement over the previous system. It was possible to carry out tests throughout the velocity range. Even though the stiffness of the bridge itself was adequate, the torsional rigidity of the drive shafts reduced the theoretical values of the lowest natural frequency of the bridge to below 5.6 Hz and reduced the measured value to 2.5 Hz. Unfortunately this frequency is in the range of interest for the test pile and interferes with the resulting ice force. With the low velocities in some tests the ice velocity was not constant but included a carriage vibration component. For future tests it may be better to make the test pile more flexible and the ice weaker to minimize the effect of carriage flexibility on the ice force.

ICE PROPERTIES

Scaling down the ice properties required that all the parameters affecting the studied phenomenon be correctly taken into account. During studies of ice crushing against a pile, geometric similitude of the pile diameter, the thickness, strength, stiffness and failure patterns of the ice, and the grain size and structure are necessary.

Six ice fields were frozen and tested in the test basin during December 1979 and January 1980. The first was just for cleaning the dust and dirt from the water surface of the tank. The instrumentation was tested as this ice sheet was pulled across the basin. The second ice field was made of freshwater ice. The seeding was done with a water spray; the results were poor, with several patches of ice having uncontrolled large crystals. The freshwater results are therefore not reliable.

The use of urea instead of natrium chloride to scale down ice properties has been shown to be promising in laboratory tests.[18] To avoid the severe corrosion problems with salt, urea was used. For about a 1:10 reduction in ice strength a 0.6% urea concentration was chosen for use in the next four ice fields. This appeared to be a good choice.

To produce the urea-doped ice the seeding was done using steam at an air temperature of -15°C, yielding fine initial grains. About 15 mm from the top a columnar-grained ice with a horizontal c-axis started to grow. As crystallographic studies show (Fig. 6), the urea ice is similar to sea ice, fulfilling the geometric similitude requirement. The cracking patterns (radial cracks both longitudinal and 20-40° off the centerline) were typically similar to those of

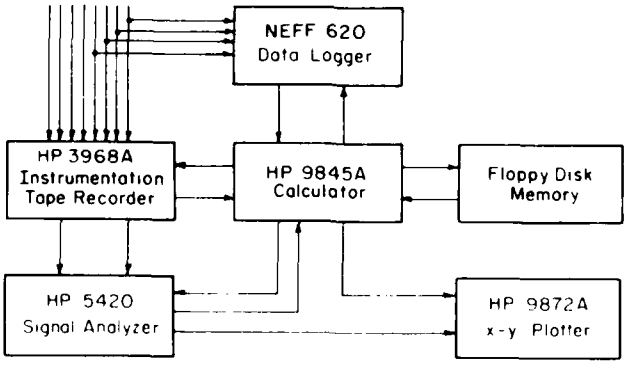

Figure 5. Signal recording and processing equipment.

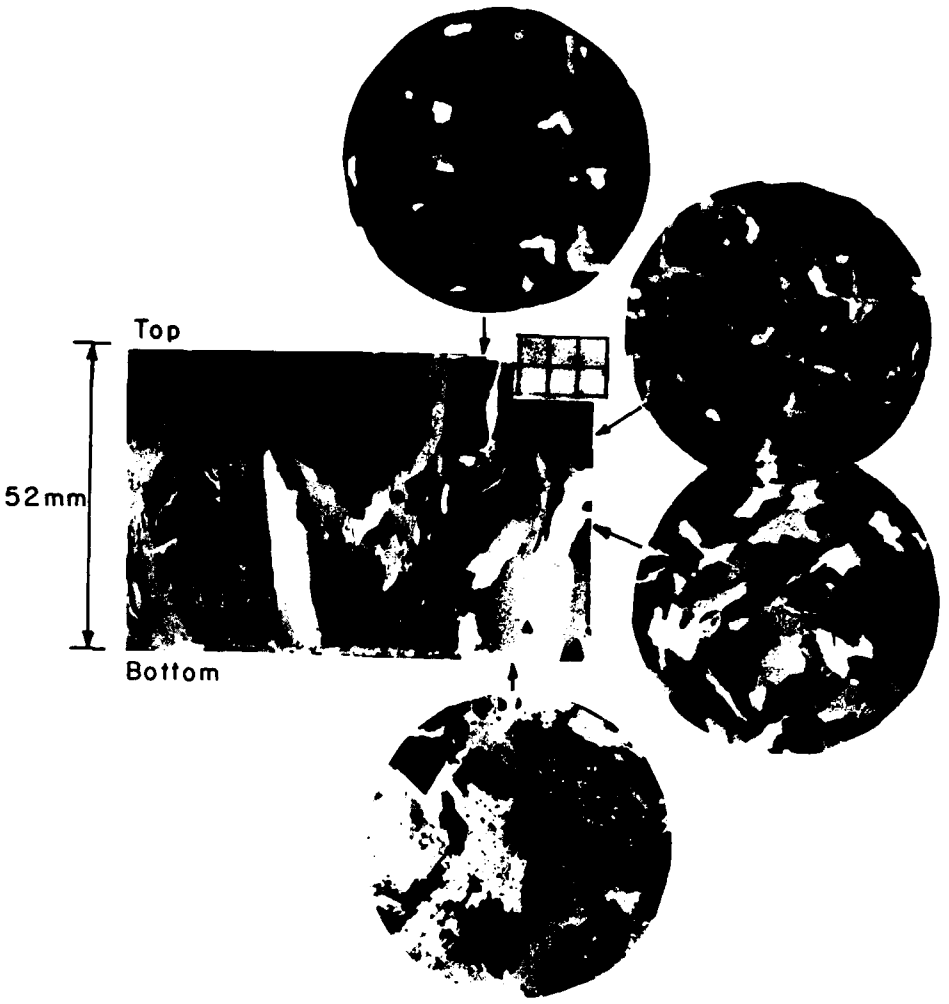

Figure 6. Vertical cross section (rectangle) and horizontal cross sections (circles) of 0.6% urea ice (tests 37–40). The grid size is 5×5 mm.

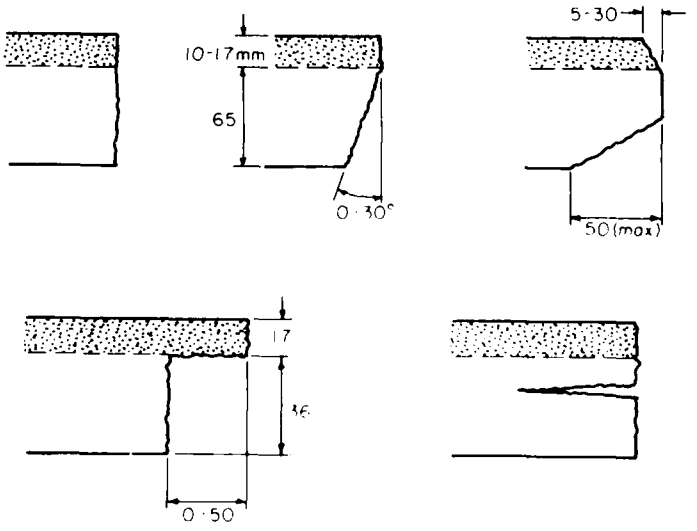

Figure 7. Crushing track cross sections.

saline ice. Also, the cross sections of the crushing track (Fig. 7) were similar to those of saline ice. However, it appears that ice thicknesses well above 20 mm should be used so that the proportion of columnar crystals will be sufficient. The strength of urea ice reduces during the warm-up period, which has to be longer than with saline ice.

For crushing, the best measure of strength would be plane compressive or shear strength. Due to the lack of procedures for testing these properties, standard cantilever beam flexural strength and plate bending tests were used as index tests.[21] The ice was warmed by keeping the air temperature at -1°C until the required flexural strength was achieved. Then the crushing test with a model structure was started; the crushing strength was calculated from the measurement data. The warm-up period from an ambient temperature of -15°C usually took about six hours. The E/σ_f (modulus of elasticity/flexural strength) ratio remained well about 2000. The infinite plate bending modulus of elasticity tests were in the process of being developed; the displacement transducers were located too far from the load actuator. Therefore, the modulus of elasticity values are not very accurate, and there were no measurements at all for the last two ice fields.

Table 1 gives the main properties of the ice fields in these tests. Note that the thinner ice was stronger than the thicker ice. Ice sheet 15 was the weakest and ice sheet 16 was the strongest in crushing, even though the differences in bending strength were small. This occurs with urea ice because the top layer of fine, randomly oriented ice crystals dominates flexural strength, while the whole thickness is as important in crushing. During warm-up the strength in the columnar section deteriorates faster than in the randomly oriented section. The columns start to get loose from each other, and the ice crushes easier. This phenomenon is also observed in the laboratory with sea ice.

CRUSHING PATTERNS

Dynamic ice-structure interactions appeared in each of the tests. Especially good repetitive ice force fluctuations were achieved with urea ice. The freshwater ice exhibited more randomness, evidently due to its more brittle nature. As the velocity of ice increased, the force fluctuation pattern changed significantly.

Table 1. Ice properties in tests 32-51.

Ice no. (% urea)	*Test no.*	*Pile diameter (mm)*	*Ice thickness (mm)*	*Ice temperature (°C)*	*Flexural strength (kPa)*	*Modulus of elasticity (GPa)*	*Crushing strength (MPa)*	*Notes*
11	32	102	30	-		-		Layer of dust above water
(0.0)	33	102	30	-		-		
12	34	102	35	-0.2			3.26	Partly unsuccessful seeding
(0.0)	35	178	38	-0.1	830	-	1.69	by water spray
	36	64	38	-0.1			3.30	
	37	64	50	-1.0			0.94	Some fluctuations of air
13	38	102	51	-0.8	150	3.90	0.80	temperature during freezing
(0.60)	39	178	52	-0.6			0.92	-20°C ... -10°C
	40	178	53	-0.4			0.86	
	41	178	53	-0.9			0.97	Severe fluctuations of air
14	42	102	53	-0.8	120	3.20	1.07	temperature during freezing
(0.60)	43	102	54	-0.8			1.36	-20°C ... -4°C
	44	178	55	-0.7			1.02	
	45	102	79				0.71	
15	46	178	79		160		0.71	
(0.60)	47	178	79				0.64	
	48	64	82				0.69	
16	49	64	22				1.43	
(0.60)	50	102	21		150		1.48	
	51	178	20				1.53	

At low speeds a sawtooth pattern formed. The ice edge stuck to the pile and deflected it with almost the velocity of the ice movement. The low loading rate initially caused ductile failure of the ice, but the spring-back rate of the structure as the ice failed by crushing made the failure brittle. Due to the inertia of the structure the spring-back exceeded the equilibrium position. After the maximum spring-back the pile started to spring forward in the direction of ice movement. At low ice velocities the spring-forward rate was higher than the ice velocity, causing the structure to pull away from the ice. Shortly, however, the edge of the ice hit again, causing another cycle of crushing and separating. Because the ice properties were random, these loading cycles varied; however, the overall patterns remain the same. Good examples are the constant ice velocity test 40 (Fig. 8a) and a sample of test 44 (Fig. 8b).

With the increasing ice velocity the sawtooth pattern persisted but included more randomness. After the spring-back the following spring-forward rate no longer exceeded the ice velocity; thus, the contact between ice and structure was continuous, and the ice force no longer dropped to zero after crushing. During the ice force build-up the loading rate can still cause ice failure in the ductile range, even though the ice velocity alone would make the failure brittle. The deflection rate of the pile affects the relative velocity between the ice and pile, and it is this relative velocity that determines the momentary loading rate.

The average ice velocity has its effects, of course. The maximum ice forces usually occurred at the low ice velocities corresponding to the ductile loading rate. In some instances the maximum ice forces appeared at the high velocities corresponding to the brittle loading rate. Whether this was a result of randomness in ice strength and contact or still a result of low relative velocity is difficult to judge. In most cases the high ice force at the beginning of the test was due to better contact between the ice and the pile than after crushing caused random contact areas.

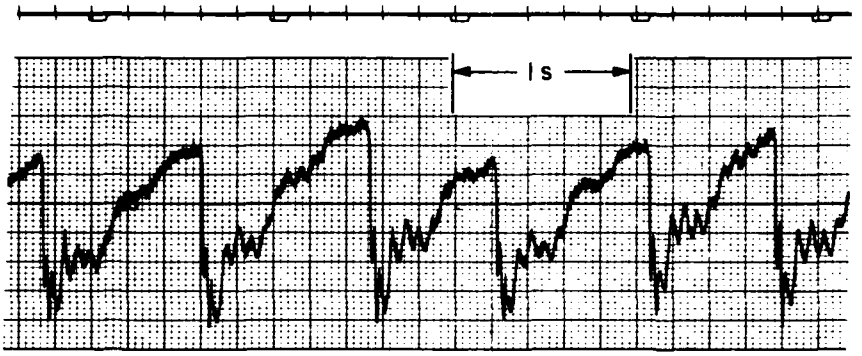

a. Test 40 (V = 11 mm/s).

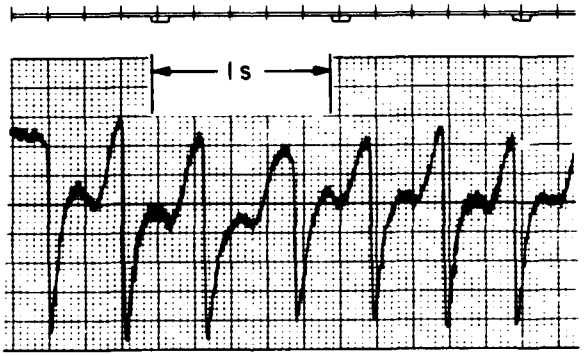

b. Test 44 (V = 16 mm/s).

Figure 8. Ice force vs time.

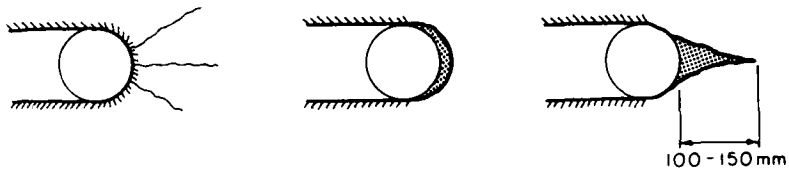

Figure 9. Crushing tracks and cracking patterns from above.

The failure of the ice before the circular pile caused radial cracks to propagate. Only in test 41 were circumferential cracks observed. Longitudinal cracks were the most common, but cracks aligned 20-40° aside were also frequent. The lengths of the cracks were from 0.3 to 3 meters. The longest one split the ice field into two parts. In a few cases transverse cracks formed on both sides of the test pile, cutting the moving ice field. The cracks apparently had little effect on the ice crushing itself. The measurement data also give no clear indication of the reduction in ice forces due to cracks. The obvious explanation for this reduction is that the edges of the test basin confined further lateral movement of the ice, and thus the only way for ice to pass the pile was to be crushed.

Further details of the ice failure process in crushing were studied by taking a 16 mm film. The results were not satisfactory, and more information was gained by observing the cross sections of crushing tracks and broken pieces of ice directly. Figure 7 shows the cross sections of the crushing tracks; Figure 9 shows some top views.

The most common crushing track for freshwater ice was tapered. The taper angle was not constant but varied randomly from vertical to 30° and on a few occasions to 45°. Wedged cross sections also appeared frequently. The width of the track was almost exactly the same as the width of the pile. The edges at the narrowest point of the cross sections were smoothed because the ice yielded under pressure against the sides of the pile.

The crushing tracks of urea ice were mostly similar to those of freshwater ice. A different feature was a lipped track, which also occurs in saline ice. This pattern resulted from the deterioration of bonds between columnar grains during the warm-up period before the tests. During crushing, as the crushed ice rubble was pushed aside, it loosened entire columnar grains instead of splitting them as in the more common tapered pattern. In rare cases the ice split at the center. If the horizontal center crack developed in the zone of transition from randomly oriented ice crystals to columnar grains, it would create the lipped crushing track. In the wedged track, wedges extending up to 50 mm were split randomly from both upper and lower surfaces.

Top views of the crushing patterns are shown in Figure 9. The most common type had radial cracks; however, sometimes no radial cracks were present and in some cases a wedge of ice in front of the pile crushed into small pieces at once. There was no correlation between the cracking patterns and ice velocity. With thin ice, wide diameter pile and low velocity, ice failed by buckling (tests 50 and 51). The pieces of crushed ice were usually very small, typically below 5 mm; only the wedges of the type shown in Figure 7 were larger.

All of these crushing and cracking patterns except the lipped crushing track have been observed in the field by the author. This confirms the usefulness of laboratory tests in simulating ice crushing against piles.

MAXIMUM ICE FORCE VS VELOCITY

Table 2 is a compilation of the maximum recorded ice forces and their corresponding velocities. The ice forces are refined from the dynamic inertial effects of the superstructure by using the bending moment and shear force measurements above the waterline in the test pile. An error, smaller than that of the superstructure effects, remains and is attributed to the inertial effects of the structures below the waterline. In tests 34, 35 and 36, a floppy-disk memory error makes the data unreliable for velocities over 20 mm/s.

The data show that half of the maximum occurred in the low velocity range and half in the high velocity range. However, the overall number of occurrences in each test in the low velocity range is more frequent. At high velocities the ice force is more random, and only when a combination of correct dynamic amplification rate, good ice contact and high ice strength occur will the resulting ice force exceed the ice forces in the low velocity range. Considering the average of averaged ice forces, there is a reduction of 38–45% from low to high velocity and a reduction of 11–14% for average of maximums in tests 37–44. For tests

Table 2. Maximum ice force vs velocity.

Test number	F_{max}* (kN)	v at F_{max} (mm/s)	$F_{av\ max}$ (kN)	v at $F_{av\ max}$ (mm/s)	F_{std} (kN)
34	19.3	18	8.2	17	5.7
35	16.2	108	2.6	14	1.9
36	15.7	102	2.0	18	0.9
37	6.6	11	5.3	9	0.9
38	9.1	30	4.9	14	1.3
39	14.5	11	7.1	9	4.3
40	14.4	12	9.6	6	2.4
41	14.5	16	9.1	18	3.2
42	11.5	27	7.5	18	2.4
43	16.1	5	8.7	9	4.5
44	15.9	66	7.9	9	3.0
45	16.0	~60	6.3	~37	2.2
46	18.0	71	6.5	21	3.7
47	17.7	98	6.2	63	3.3
48	9.7	90	~6.6	11	-
49	3.3	31	1.8	8	0.5
50	4.4	93	1.2	4	1.1
51	6.6	94	2.3	30	1.2

*F_{max} = maximum in the test, $F_{av\ max}$ = maximum average ice force, F_{std} = standard deviation of ice force.

45-51 the reduction of averages is only 9-15% but the maximums increase 13-21%.

The fourth and fifth columns of Table 2 show the maximums of the averaged ice forces and their velocities for each 3.15-second interval of data collection. This time period is long enough to include several ice force cycles but short enough to show the changes with increasing velocity. (The graphic output of this data is given in Appendix A.) The standard deviations and the maximum values during each 3.15-second interval are given. In the case of the maximum of the averages the corresponding ice velocity is always low and matches the transition zone from ductile to brittle loading rate.

An apparent discrepancy with the theory of self-excited, ice-induced vibrations is that the pile diameter does not affect the velocity of the occurrence of maximums. The stress rate definition[1] is

$$\dot{\sigma} = \frac{8\sigma_c \nu}{\pi D} \qquad (1)$$

where σ_c is the crushing strength, ν is the ice velocity and D is the diameter of the pile, to which the stress rate is inversely proportional. Because the stress rate corresponding to the transition from ductile to brittle should be the same in the same ice field, the change of pile diameter from 64 to 178 mm should have increased the relevant velocity 2.8 times. There is a small indication of this trend between tests 37 and 39, but elsewhere the results are independent. In tests 50 and 51 the initiation of buckling prevents comparisons to test 49. A possible explanation for the independence of the pile diameter is that during pile vibrations the relative velocity between the pile and the ice is lower during the force build-up phase than it would be with a stiff structure with ice velocity alone. Thus the same stress or strain rate can be achieved in a wide velocity range, or inversely, the same stress rate can be achieved with the same velocities but with different diameters.

Another factor is the aspect ratio (pile diameter at waterline/ice thickness) effect. With larger diameters the aspect ratio effect is smaller, and as effective crushing strength should be used in eq 1, it tends to reduce the diameter effects. If this is taken into account, the ratio of 2.8 between tests 37 and 39 reduces to 2.0. The questions, "How does the ice in front of the pile feel this aspect ratio effect and how is this accounted for in the stress rate equation?" are still unanswered.

Appendix B shows that the standard deviation of the ice force follows quite closely the behavior of the averages with increasing velocities. The maximum standard deviations occur in the area of transition from ductile to brittle ice and decrease thereafter. The ratio of the average to the standard deviation is usually around 0.5, but it varies from 0.2 to 0.8. In test 43 the ratio is near 1.0, but it appears that the initial zero for calculation was 1.7 kN; this value should be added to both the average and the maximum

readings in that test. Thus, the correct ratio in test 43 is around 0.47. In tests 34, 35 and 36 the standard deviations are higher than average; however, this is probably a result of errors in storing data on the floppy disk.

If a short sample of the ice force history is available, the maximum ice force can be estimated with the following equation

$$F_{max} = F_{av} + 3 \cdot F_{std} . \quad (2)$$

Equation 2 is commonly used in statistical analysis in predicting maximums for normally distributed samples. A further study is planned to figure out what kind of statistical distribution the measured ice forces follow. The coefficient 3 corresponds to a 99.9% confidence limit. Equation 2 predicts the maximums well for the whole velocity range in Appendix B. In design, therefore, it is better to estimate the maximum ice force using eq 2 than to use a measured maximum value directly.

DYNAMIC ASPECT RATIO EFFECT AND CRUSHING STRENGTH

The effective ice pressure against a vertical pile depends on the pile diameter to ice thickness ratio. A great many reports of model studies and in a few cases of full-scale measurements have indicated that the ice pressure against an infinite pile has to be multiplied by a factor κ to get an effective pressure against a finite width pile:[16]

$$\kappa = \sqrt{1 + 5\,H/D} \quad (3)$$

where H is the ice thickness and D is the pile diameter at the waterline. Earlier model tests have been more or less static and have had a relatively short stroke of the test piece into the ice. In this test series, in addition to varying the ice thickness and the pile diameter, the ice velocity was varied throughout the range from ductile to brittle failure mode, and no limitation was present due to the length of the ice fields. Thus, the dynamic aspect ratio effect during continuous crushing could be measured.

Table 3 gives the average and maximum ice forces and the effective crushing strengths for the low and high velocity ranges. The low velocity corresponds to the area of transition from ductile to brittle ice, and the high velocity corresponds to the brittle range, with the possibility that the pile deflection rate may cause ductile loading rates during force build-up. For better comparisons the 3.15-second samples are chosen from the same velocity range as much as possible. Exceptions are due to the small effect of longitudinal cracks and in tests 50 and 51 to buckling, which reduced the ice loads significantly in the low velocity range. Computer data for tests 34–36 are unreliable for velocities above 20 mm/s. The tests for each ice field usually took 1–2 hours, so the ice in the last tests was tempered longer and thus was weaker.

Table 3. Effective crushing strength at low and high velocities.

				Low velocity					*High velocity*				
Test number	D *(mm)*	H *(mm)*	κ*	v *(mm/s)*	F_{av} *(kN)*	F_{max} *(kN)*	σ_{av} *(kPa)*	σ_{max} *(kPa)*	v *(mm/s)*	F_{av} *(kN)*	F_{max} *(kN)*	σ_{av} *(kPa)*	σ_{max} *(kPa)*
34	102	35	1.65	17	8.2	19.3	1390	3260	90	-	10.0	-	1690
35	178	38	1.43	15	2.6	7.1	270	740	90	-	13.2	-	1380
36	64	38	1 99	17	2.0	4.5	420	940	90	-	10.6	-	2230
37	64	50	2.22	11	4.2	6.6	590	940	71	2.6	5.8	370	820
38	102	51	1.87	14	4.9	8.5	510	880	76	3.3	8.9	340	910
39	178	52	1.57	11	7.1	14.5	490	990	73	4.8	11.6	330	800
40	178	53	1.58	12	9.4	14.4	630	970	-	-	-	-	-
41	178	53	1.58	16	9.0	14.5	610	970	75	4.8	12.2	320	820
42	102	53	1.90	14	6.4	10.7	630	1050	76	3.6	10.0	350	980
43	102	54	1.91	11	6.7	10.7	640	1020	74	3.4	8.1	320	770
44	178	55	1.60	9	7.9	12.8	500	820	74	4.9	11.5	310	740
45	102	79	2.21	22	5.7	13.9	320	780	70	5.4	16.0	300	900
46	178	79	1.80	20	6.5	13.3	260	520	70	5.8	18.0	220	710
47	178	79	1.80	39	5.3	15.0	240	570	63	6.2	16.3	240	640
48	64	82	2.72	24	5.5	7.9	390	560	90	3.8	9.7	270	690
49	64	22	1.65	8	1.8	2.9	780	1260	80	0.9	2.6	390	1130
50	102	21	1.42	4	1.2	3.2	400	1070	80	1.4	3.5	470	1180
51	178	20	1.24	5	1.3	3.7	300	860	70	2.1	5.5	490	1280

* $\kappa = \sqrt{1 + 5\,H/D}$; av = average in 3.15-s interval; max = maximum value; $\sigma = F/\kappa DH$.

The results show that the effective ice pressure can be predicted quite well by using the aspect ratio effect (eq 3). The calculated crushing strengths against an infinitely wide pile given in Table 3 for different diameters are relatively close to their average in the same ice field. Even the results from ice fields 13 and 14 (tests 37–40 and 41–44) are almost identical in spite of the dynamically different structural configurations. Even though the deviations of crushing stresses in each ice field are within the expected range, there is a trend that suggests that the aspect ratio effect could be stronger than according to eq 3.

The crushing strength decreased with increasing thickness of urea ice. The explanation is that the proportion of surface layer of ice with a vertical c-axis is much larger with thin ice than with thick ice. As all ice fields had roughly the same bending strength, it appears that the surface layer does not lose its crushing strength as fast as it lost its bending strength during tempering.

In these tests the ratio of crushing strength to bending strength is about 6 for maximum values and about 3 for average values. This is the same ratio as for full-scale ice strengths. The scale reduction of strength due to urea-doping and tempering is about 5 for a full-scale flexural strength of 800 kPa, about 3 for maximum and about 6 for average crushing strengths if a value of 2800 kPa is adopted for the full-scale strength. During the six-hour tempering the flexural strength reduced by half, the rest of the reduction being due to urea. No tests were conducted to determine the reduction rate of the crushing strength during tempering.

MEASURED ICE FORCE FREQUENCIES

One of the main objectives of these tests was to create continuously repeating ice force fluctuations under controlled conditions. In most tests there are good examples of how the ice force repeats itself with similar patterns and how the velocity of the ice changes both the shape and frequency of ice force fluctuations. In test 40 the ice velocity was kept constant, and it was chosen to give the maximum amplitude. A repeating force and displacement pattern developed (Fig. 8a). The vibrating pile reached its limit cycles. Only the randomness in ice strength created the small variations.

The frequency of the ice force fluctuations depended on the ice velocity and the natural frequencies of the structure. The effects of pile diameter and ice thickness were also present. Table 4 includes the dominant frequencies of ice forces with different velocities in those tests that exhibited distinct ice force fluctuations. The frequencies were measured directly from the force-time histories. The signal analyzer was not used to solve for the low frequency components because both long sampling periods and several averages would have been required, which would have reduced spectrum peaks, as the frequency was continuously changing with increasing ice velocity. Only the low velocity range frequencies are given in Table 4, and they are the local values for only one or two loading cycles that best present the ice force fluctuations for each velocity point.

Plotter graphs (Appendix C) and Table 4 indicate that the crushing frequency increases at the same rate as the ice velocity at the beginning and then starts to lag at velocities over 20 mm/s. Over 30–40

Table 4. Crushing frequency at low velocity range. During each test three samples were taken as the velocity increased.

	Sample 1					*Sample 2*					*Sample 3*				
Test number	v* *(mm/s)*	f *(Hz)*	F *(kN)*	f_0 *(Hz)*	f/f_0	v *(mm/s)*	f *(Hz)*	F *(kN)*	f_0 *(Hz)*	f/f_0	v *(mm/s)*	f *(Hz)*	F *(kN)*	f_0 *(Hz)*	f/f_0
38	10	1.0	6.7	3.5	0.29	16	2.1	7.4	5.0	0.42	27	2.1	8.1	7.8	0.27
39	10	0.44	14.6	1.5	0.29	16	1.3	10.2	3.7	0.36	27	2.3	10.3	6.1	0.38
40	12	0.91	14.4	1.9	0.47	22	2.4	10.6	5.0	0.48	-	-	-	-	
41	14	0.96	13.2	2.5	0.39	19	1.5	14.1	3.1	0.48	35	2.1	13.9	5.9	0.36
42	7	0.67	7.2	2.3	0.30	18	1.6	10.1	4.2	0.48	25	2.0	10.5	5.6	0.30
43	11	0.82	10.7	2.4	0.34	19	2.1	7.8	5.7	0.39	29	2.2	8.0	8.5	0.26
44	9	0.48	12.9	1.6	0.30	17	1.2	12.9	3.1	0.37	26	2.3	10.8	5.6	0.41
Average	10				0.34	18				0.43	28				0.33

* v = ice velocity, f = measured frequency,
F = ice force, f_0 = calculated frequency from eq 5.

mm/s the crushing frequency jumps intermittently to 8.5 Hz, which is the lowest natural frequency of the pile, and then remains at 8.5 Hz as the velocity further increases, even up to maximum velocity (110 mm/s). In tests 43 and 44 the velocity range during which crushing frequency follows ice velocity was below 20 mm/s; above that, a frequency varying from 2.2 to 2.8 Hz was dominant up to 63 mm/s in test 43 and up to 95 mm/s in test 44. Thereafter the crushing frequency increased again with velocity. The first natural frequency of the pile was 2.6 Hz and that of the carriage was 2.5 Hz. The next natural frequency of the pile in tests 43 and 44 contributing significantly to the deformation of the pile at the waterline was 37.5 Hz. It appears that the natural frequencies attract crushing frequencies. This proves that the response of the structure (in addition to ice itself) affected the resulting ice force.

In tests 38–44 the ice thickness was 53±2 mm, and the stiffness of pile in the direction of the ice force was constant. A parameter that is equally as important for crushing frequency as ice velocity is the magnitude of the ice force, or more specifically, the range of the ice force during repeating loading cycles. Table 4 verifies that crushing frequency is inversely proportional to the ice force.

CALCULATED ICE FORCE FREQUENCIES

There are two reported methods for predicting the frequency of the ice force during crushing. Neill[16] explained that ice has a tendency to fail into floes of a certain size, 0.2–0.5 times the ice thickness. This yields the equation

$$f = 2\,\frac{v}{H} \;\ldots\; 5\,\frac{v}{H} \quad . \tag{4}$$

Another method[12] starts from the length of ice that is crushed during each cycle. If it is equal to the elastic displacement of the structure with the maximum ice force just before crushing starts, then

$$f = \frac{kv}{F} \tag{5}$$

where k is the stiffness coefficient of the structure toward the direction of ice action at the ice action point. If the ice forces do not reduce to zero during the crushing phase, the range of the ice force should be used instead of the maximum. In dynamic conditions the magnification factor should be applied to the ice force to account for the increasing crushing lengths.

If eq 4 is used to predict the low crushing frequencies in Table 4, it succeeds in all but three of the intermediate velocity cases. However, it falls short of predicting the constant frequency of 8.5 Hz (all the tests except 43 and 44). In tests 43 and 44 the frequency of 2.5 Hz can be predicted, but only with an unrealistic assumption that the coefficient 0.2–0.5 in the denominator should be velocity dependent. In the tests the crushed or failed ice pieces were never larger with higher velocities. Also, in tests 43 and 44 eq 4 fails to predict crushing frequencies over 15 Hz.

The columns for f_0 in Table 4 present the crushing frequencies calculated using eq 5. It appears that the prediction is always too high. It should be somewhat higher because eq 5 takes into account only the time for load build-up, not the crushing phase. However, from plotter graphs it can be seen that the crushing phase is very short, and thus its contribution to crushing frequency is negligible at low velocities. Another factor is that the inertia of the structure may make the crushed distance longer than the static displacement F/k in eq 5.

The ratio of measured to calculated frequencies averaged from 0.33 to 0.43 with relatively small deviations. As both velocity and ice force in eq 5 are measured quantities, a reduction coefficient should be applied to the pile stiffness k. As ice is pushed by the test carrier bridge, the stiffness of the bridge, frames, ice boom and ice also have to be taken into account. These stiffnesses are 17.2, 155, 19.5 and 112 kN/mm, respectively. In series with the pile stiffness of 2.33 kN/mm, the overall stiffness is 1.80 kN/mm, yielding a reduction coefficient of 0.77. In addition, gaps in the ice boom joints and frame connections decrease the stiffness further.

The effective stiffness of the pile against the ice force can be calculated from plotter graphs using the definition of stiffness:

$$k = \frac{F}{x} = \frac{\Delta F}{\Delta x} = \frac{\Delta F}{v \cdot \Delta t} \quad . \tag{6}$$

During the load build-up phase a sample taken over a time of Δt is chosen that yields a displacement $v \cdot \Delta t$ and an increase in ice force ΔF. Table 5 provides data for calculating effective stiffnesses in some tests.

Straight load build-up in plotter graphs exist only at low velocities. The loading rate is then so low that viscoelastic yielding increases the deformations in ice and thus decreases the calculated stiffness values, because velocity v in Table 5 is ice velocity and not the relative velocity between the ice and the structure. Another factor is the contact coefficient. The less area of pile that touches the ice, the higher the local ice pressures and displacements and the lower the effective stiffness.

The frequency ratios in Table 4 coincide with the stiffness ratios in Table 5, recognizing the viscoelastic

Table 5. Calculation of effective stiffnesses.

Test number	Δt (s)	v (mm/s)	ΔF (kN)	k_{eff} (N/mm)	k_{eff}/k_{pile}
39	3.0	4.6	8.0	580	0.25
39	2.0	9.0	15.0	840	0.36
40	3.3	3.9	10.3	800	0.34
41	3.0	9.7	11.7	400	0.17
42	3.0	4.2	6.5	520	0.22
42	2.0	8.8	7.2	410	0.18
43	3.0	4.2	11.1	880	0.38
44	2.0	4.5	5.9	660	0.28
44	1.0	8.9	4.5	500	0.21
44	2.0	4.6	6.6	720	0.31
			Average	630	0.27

effects in the latter. The measurements of frequencies correlate well with the values predicted by eq 5; the correct frequencies can be predicted by using the effective stiffness instead of the pile stiffness alone. In addition the frequency ratios according to eq 5 are lowest at low loading rates, where viscoelastic effects are pronounced; they reach a maximum as load build-up time shortens and then decrease at increasing velocities as the time for deflection springback becomes more significant. This measured dependence was predicted earlier using computer simulations.[15]

Equation 5 also neatly explains why the natural frequencies of the structure can persist in the ice force for a wide velocity range. The range of ice force and the length of the crushed ice are increasing with velocity, while the frequency can remain constant. For example, in test 41 the first natural frequency of the pile (8.5 Hz) appears at 40 mm/s velocity and persists up to the maximum velocity of 85 mm/s. The range of the ice force without dynamic correction at 40 mm/s is 4 kN and at 85 mm/s, 8 kN. If the effective stiffness is 850 N/mm, the crushing length increases from 4.7 to 9.4 mm.

Peyton[14] measured ice force frequencies at Cook Inlet with a full-scale structure that had the first natural frequency around 1.0 Hz. Because measurements under varying conditions yielded a crushing frequency of about 1 Hz, he concluded that it is a physical property of ice to fail at this frequency during crushing. In the present tests, 8.5-Hz vibrations also prevailed at varying ice thicknesses and velocities. However, when the structural configuration was changed and there was no dynamically unstable natural mode at 8.5 Hz, ice-induced vibrations no longer appeared at this frequency. This proves that the crushing frequency is not a property of ice alone but is also the result of the structural properties in a dynamic ice-structure interaction.

A signal analyzer was used to calculate the 8.5-Hz vibration amplitudes (Fig. 10). In tests 37–42 the

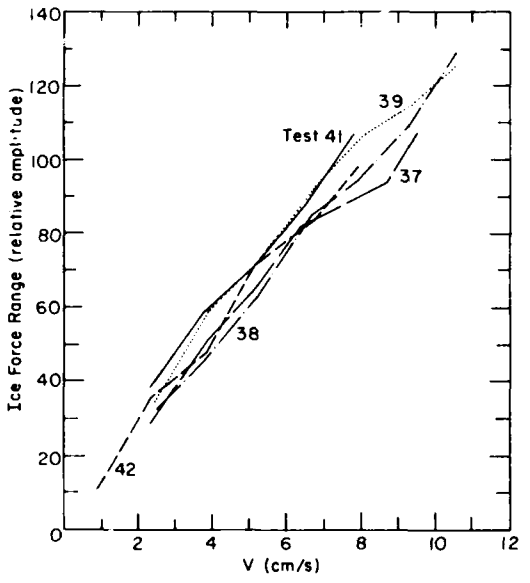

a. Tests 37–42.

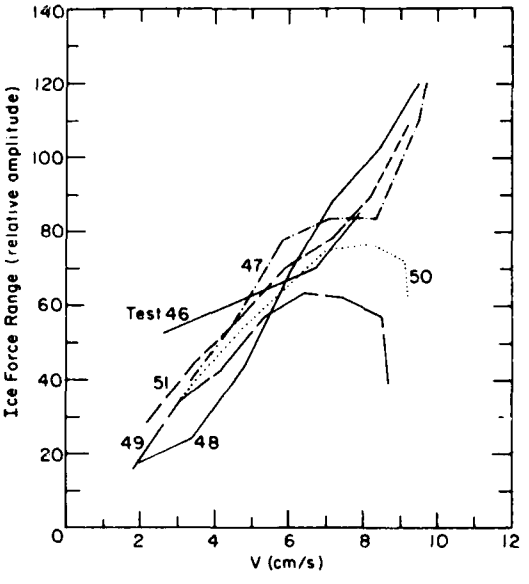

b. Tests 46–51.

Figure 10. Ice force range at 8.5 Hz vs velocity (ice force without dynamic correction).

pile diameter had no apparent effect on the vibration amplitudes. Theoretically when stress rate effect is taken into account, there is no direct dependence on diameter either.

Substituting the velocity from eq 1 and the ice force components into eq 5 results in

$$f = \frac{k \cdot \frac{\pi D \dot{\sigma}}{8\kappa\sigma_c}}{\kappa\sigma_c HD} = \frac{\pi}{8} \cdot \frac{k}{\kappa^2 \sigma_c H} \frac{\dot{\sigma}}{\sigma_c} \qquad (7)$$

which shows that the diameter has its effect only through the square of the aspect ratio coefficient κ. The aspect ratio effect κ is taken into account also in the stress rate (eq 1), because σ_c in eq 1 is the maximum elastic stress in the ice in front of the pile. In tests 45-51 the ice thickness was changed, and Fig. 11b shows that there is not much change in amplitudes compared to tests 37-42. The reason is that the crushing strength is lower with thicker ice and higher with thin ice than in tests 37-42 (Table 3). This, together with the aspect ratio effects, results in small changes in crushing frequencies, or inversely, in crushing amplitudes, because the frequency is constant because the natural frequency of the structure dominates.

A significant change in crushing amplitudes occurred in tests 49 and 50. With thin ice the ice force fluctuations were small, and when the velocity was high enough, eq 5 predicted higher frequencies than the natural frequency of 8.5 Hz. With increasing velocity the amplitudes first increased as long as the undisturbed frequency remained below 8.5 Hz and reduced thereafter. The undisturbed frequency is the crushing frequency that would prevail if the natural frequency of the pile did not dominate the response; compare the low velocity frequencies in tests 43 and 44 (Table 4). Thus, as frequency is constant, a resonance-like condition appears in the amplitude response. In test 50 the diameter was wider, requiring a higher velocity for resonance. For test 51 the resonant velocity was beyond the test velocity range. With the thick ice in tests 37-42 and 45-48 the velocity never reached resonance with 8.5 Hz.

As the velocity increased over 84 mm/s in test 49 and over 92 mm/s in test 50, the second natural frequency (60 Hz, but not AC noise; compare Fig. 4) started to appear in the ice force. For short periods the first mode disappeared and the response was almost entirely second mode. Again eq 5 gives the correct frequency, with the measured ice force range of 1 kN and effective pile stiffness of 850 N/mm.

In tests 43 and 44 the first two natural frequencies of the pile were 2.6 and 37.5 Hz. According to stability theories for ice-induced vibrations, the 2.6-Hz mode should be stable and should not be excited by the ice crushing. The averaged power spectrums indicate that this is the case in test 43. There is some excitation in the first superstructure mode up to 100 mm/s, but resonance never occurs.

In test 44 the only difference was the pile diameter, which only increases the ice forces when the dynamic behavior of the pile remains unaltered. In this test, however, continuous high-level vibrations occurred in a frequency range of 2.2-2.8 Hz, while the ice velocity was between 35 and 75 mm/s. The most persistent vibrations occurred at 2.5 Hz, and the maximum amplitudes were recorded at a velocity of 60 mm/s, which can be regarded as a resonant point. The analysis of ice force and acceleration waveforms revealed that it was not a resonance with the test pile, since the phase shift with the ice force and pile acceleration is 142°; more likely it is a resonance with the carriage, for which the phase shift is 112° (Fig. 11). This condition prevailed in the whole velocity range from 35 to 75 mm/s for which 2.5-Hz vibrations were continuous. In tests for the carriage alone the natural mode with a frequency of 2.5 Hz was measured. It appears that the flexible carriage and ice field is a mechanical system that is excited by the ice crushing. This system is dynamically unstable and is the reason for the resonance around 2.5 Hz. As the first natural frequencies of the test pile and carriage were almost identical, the vibrations of the test pile were also strongly amplified.

The dependence of crushing frequency and ice force amplitudes on the whole velocity range in these tests can be explained using eq 5. A similar dependence can also be predicted analytically if the dynamic response of the pile is tied together with the dependence of the ice crushing on the loading rate. Thus, it can be concluded that eq 5 is valuable in predicting crushing frequency ranges and possibilities for resonance. The natural frequencies of the structure persist in a wide velocity range, while force and displacement amplitudes change instead of frequency. Otherwise the frequencies that eq 5 predicts are always a bit too high. This is due to viscoelastic yielding at low velocities, deflection spring-back times at high velocities, and reduced effective pile-carriage stiffness. In the field the latter results only from the elastic deformations of ice and is due to uneven contact between the ice and the pile.

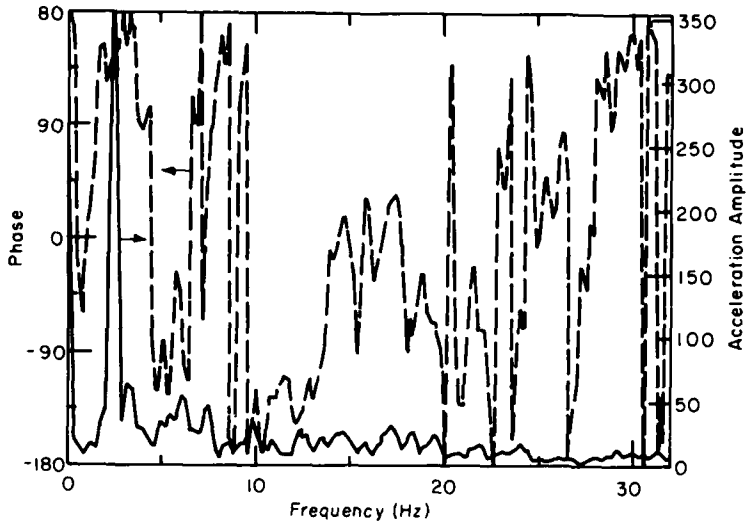

a. Test pile top acceleration phase vs carriage acceleration, and carriage acceleration amplitude spectrum.

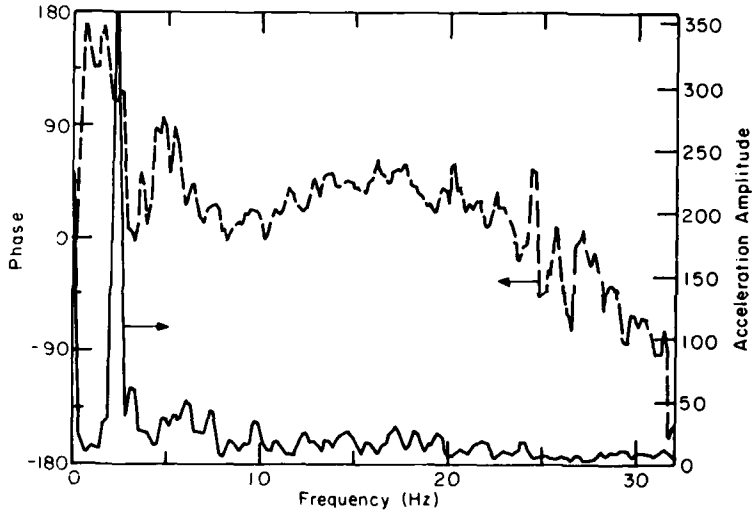

b. Carriage acceleration phase vs ice force, and carriage acceleration amplitude spectrum.

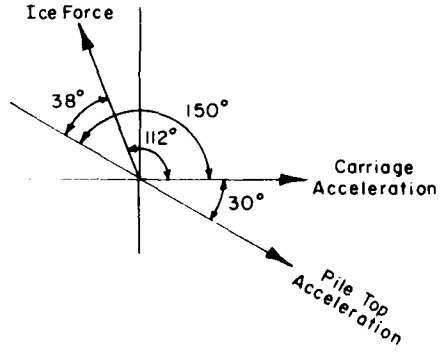

c. Phase vector diagram for ice force, pile and carriage accelerations.

Figure 11. Ice force, pile and carriage acceleration phases (test 44, v = 30–60 mm/s).

Table 6. Accelerations, velocities and displacements.

Test	v_{ice} (cm/s)	Acceleration (g)*		Velocity† (cm/s)		Displacement† (cm)		Note
		parallel	perpendicular	parallel	perpendicular	parallel	perpendicular	
37	2.0	1.2	0.4	22	7	0.41	0.14	Decaying
	10.1	3.2	2.2	59	-	1.11	-	Continuous
38	2.0	2.6	0.4	48	6	0.11	0.14	Decaying
	8.9	2.4	1.0	45	18	0.83	0.34	Continuous
	10.9	2.6	1.0	48	18	0.11	0.34	Continuous
39	1.5	2.0	0.5	37	9	0.70	0.17	Decaying
	8.7	2.0	-	37	-	0.70	-	Continuous
40	1.2	4.0	0.7	74	12	1.39	0.22	Decaying
	1.2	3.0	2.2	56	41	1.04	0.76	Continuous
41	1.8	3.6	0.5	67	9	1.25	0.17	Decaying
	8.7	2.4	2.1	45	39	0.83	0.73	Decaying
42	1.7	7.7	0.7	-	12	-	0.22	Decaying
	6.4	1.6	0.4	30	8	0.56	0.14	Continuous
43**	1.2	8.2	2.1	-	16	-	0.12	Decaying
	3.3	8.5	2.6	-	19	-	0.15	Decaying
	9.5	8.9	1.8	66	14	0.51	0.10	Continuous
44**	1.0	8.3	3.0	-	-	-	-	
	2.7	7.1	1.6	-	12	-	0.09	Decaying
	6.7	9.3	3.1	-	-	-	-	
45	≈1	6.5	0.9	-	-	-	-	
	≈6	8.5	0.7	-	-	-	-	
	≈9	<2.8	0.8	<51	-	<0.96	-	
46	2.1	8.5	1.3	-	-	≈1	-	
	7.2	8.9	2.6	<81	-	<1.5	-	
	7.2	1.5	-	28	-	0.52	-	Continuous
47	1.7	2.0	2.0	-	-	-	-	
	5.0	8.5	1.6	-	-	-	-	
	9.7	2.0	≈2.0	37	-	0.70	-	≈Continuous
48	9.0	2.4	-	44	-	0.83	-	≈Continuous
	9.8	2.4	-	44	-	0.83	-	Continuous
	9.8	2.6	1.3	48	-	0.90	-	Continuous
49	2.5	0.6	0.25	11	4.5	0.20	0.08	Continuous
	6.9	1.7	-	31	-	0.58	-	Continuous
	8.8	2.8	-	7.1	-	0.02	-	Continuous
50	2.2	0.6	-	11	-	0.20	-	Continuous
	7.8	1.4	-	26	-	0.48	-	Continuous
	9.2	2.4	-	6.1	-	0.02	-	Continuous
51	2.0	4.2	0.7	-	-	-	-	
	9.3	2.4	1.1	44	-	0.83	-	Continuous

*Acceleration in units of gravity of earth (9.81 m/s^2).

†Velocity and displacement integrations were carried out only when a distinct mode was present.

**In tests 43 and 44 longitudinal accelerations, velocities and dicplacements were measured at the top of lower structure and at the bottom of superstructure instead of parallel and perpendicular to the ice force.

ACCELERATIONS, VELOCITIES AND DISPLACEMENTS

The acceleration transducers at the superstructure were used to measure longitudinal and cross-axis vibrations in all but tests 43 and 44, where they measured the longitudinal accelerations just above and below the vibration isolation part. This measured the effectiveness of the vibration isolation. Table 6 contains the data on maximum accelerations during each test at different velocities. If the acceleration waveform is distinguishable as a single mode, then velocities and displacements were integrated. For cases of decaying vibrations the initial maximum values are given.

During the low velocity load build-up phase the acceleration was zero. During ice crushing, high frequencies from 81 to 118 Hz were present. These are higher than the two lowest natural frequencies of the structure. High frequency components die out fast, and simultaneously the first or second natural modes become dominant. The crushing is like an impact loading that excites all the natural frequencies of the structure, but only the lowest exhibit significant displacements. After crushing, the first mode vibrations die out exponentially. This first mode frequency is significantly higher than the free natural mode of the pile. As the ice edge sticks to the pile after crushing, it induces a supporting effect, which increased the natural frequency in these tests from 8.5 Hz to 12-15 Hz.

With higher velocities, when the first natural mode of the structure is able to dominate the crushing frequencies, the main waveform of acceleration is a 8.5-Hz sinusoidal curve with a second mode at 60 Hz superimposed on it. During the crushing phase even higher components are present. These induce the highest momentary accelerations. The maximum recorded values are over 9 g. In reality they have been higher, since 1) the maximum range of the accelerometers was exceeded, which caused saturation, 2) these peaks are also due to frequencies above 100 Hz and the accelerometers had natural frequencies around 100 Hz with 60% critical damping, which has an effect of a low band pass filter, 3) the data were recorded on a tape recorder with a 0-156 Hz band, and 4) the plotter attenuates amplitude peaks over 50 Hz.

Transverse vibration peaks may be as high as longitudinal ones but generally they were less than one third as high. Randomness is the main cause of transverse excitations while ice is failing first on one side at the pile and then the other. If continuous longitudinal vibrations persist, the transverse vibration remains low.

The integrated velocities at the top of the pile verify that the deformation rate of the pile can easily be much higher than the ice velocity. Considering the shape of the first mode vibrations, amplitudes at the top should be multiplied by 0.238 to get those at the ice action point. Thus, a ductile loading rate is possible over the whole velocity range. The maximum velocities are 800 mm/s at the top and 190 mm/s at the waterline. The maximum integrated top displacements are 14 mm, which, however, have been dampened.

In tests 43 and 44 the vibration isolation part dampened the vibrations in the superstructure to one third or one fourth of those at the lower structures. During the carriage resonance part of test 44 (2.6 Hz) the acceleration amplitude in the superstructure was 0.82 g. This resulted in a velocity of 493 mm/s and a displacement of 30 mm.

In tests 41-43 one longitudinal accelerometer was on the ice; in test 44 it was on the carriage. During

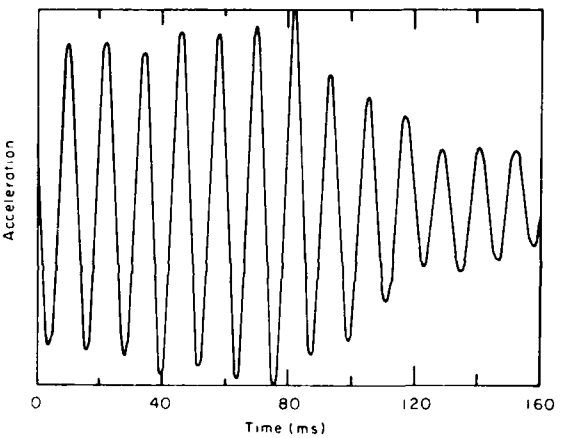

a. Ice in-plane longitudinal acceleration.

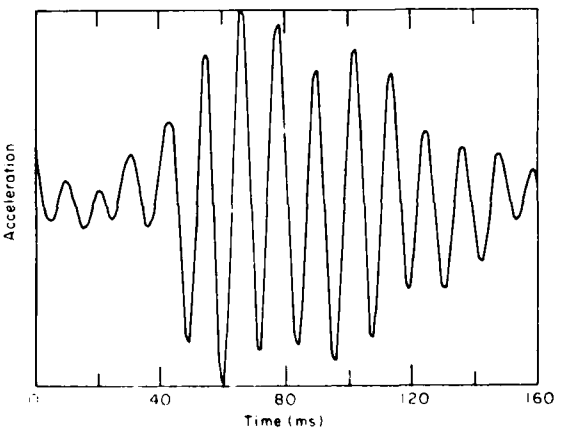

b. Carriage longitudinal acceleration at 84 Hz.

Figure 12. Acceleration during ice crushing.

the crushing phase, high-frequency vibrations over 80 Hz could be measured on both the ice and the carriage. The maximum recorded accelerations were 0.68 and 0.52 g, respectively. As previously mentioned, these peaks may have been higher but they were not recorded due to the limits of the instrumentation. Continuous vibration in the ice with 2.6 Hz caused an acceleration of 0.04 g, a velocity of 24 mm/s and displacement amplitudes of 1.4 mm. In the carriage the corresponding figures were 0.08 g, 48 mm/s and 2.9 mm.

Natural modes for 80–118 Hz vibrations enountered both in the ice and at the carriage cannot be accounted for. Not enough accelerometers were installed for identifying these modes. Either the natural modes of the carriage, the ice field in-plane vibrations, or the combination of these two were excited during the crushing phase.

Samples of high-frequency vibrations in the ice in test 43 and at the carriage in test 44 are presented in Fig. 12. In both cases vibration with a frequency around 85 Hz has started almost at the same time as crushing; thereafter the amplitudes remained at a constant level for as long as crushing lasted. This might be because the mode in question is unstable for ice-induced vibrations. Hence, limit cycles develop fast, and thereafter, only random variations in vibration amplitudes occur.

The frequency range from 80 to 118 Hz looks high, but when these scale-model tests are converted to full scale, the resulting frequency range is around 10 Hz. This is below the 15-Hz vibrations measured from a bridge pier at Pembina River.[19] With a 1:8 scale factor these model tests and the measurements at Pembina River are comparable. The ice velocity at Pembina River was higher at the beginning of crushing but then decreased to zero as ice floes in the river were stopped by the pier. The simply supported pier had a lowest natural frequency of 15 Hz and had low internal damping, which evidently made it unstable for ice-induced self-excited vibrations.

DAMPING

The damping of the test pile was measured both in and out of the water. For the first lowest natural modes there was no significant change in damping or in frequencies. At 8.5 Hz, damping was 0.8% from the critical damping, and at 60.0 Hz it was 2.7%. For tests 43 and 44 damping at 2.6 Hz was 3.2%, and at 37.5 Hz it was 7.9%. Damping at 2.6 and 8.5 Hz was measured from the decay rate of free oscillations; at other frequencies it was measured from autospectrum half-power points in conjunction with transfer function measurements using the signal analyzer. The windowing effect and weighting functions, together with averaging in the signal analyzer, broaden the peaks, resulting in considerably higher damping ratios than are measured directly from the decaying signal. Thus the signal analyzer damping ratios should be used only for comparisons.

Table 7. Damping during crushing.

Test number	A_1*	A_n	*Number of cycles*	ζ *(%)*
34	455	100	7	3.4
34	365	84	7	3.3
35	158	36	3	7.9
35	82	21	3	7.2
36	90	30	3	5.8
39	150	38	4	5.5
40	245	43	3	9.2
40	210	43	6	4.2
40	210	42	6	4.3
40	190	28	6	5.1
41	219	58	5	4.2
45	215	115	2	5.0
45	290	155	2	5.0
46	170	60	3	5.5
46	316	72	4	5.9
47	263	152	3	2.9
			Average	5.3

*A_1 = initial amplitude, A_n = amplitude after n cycles, ζ = damping factor ($\delta = 2\pi\zeta$ = logarithmic decrement).

The amount of damping during the tests can be determined either from the width of the peaks of the signal autospectrums or from the decay rates. Table 7 presents the measured dampings during the decaying vibration after crushing in low velocity range. The results show that there was a significant increase in damping (from 0.8 to 5.3%) due to the ice presence. As the main crushing had already occurred, the damping mechanism must have been due to friction between broken ice pieces and the pile and to local crushing of peaks in the uneven ice edge while a new contact developed.

There was randomness in the amount of damping. In some cases there was no significant vibration after crushing, which means that all the elastic energy of the pile had been dissipated during crushing. Similar phenomena have been observed in the field with flexible structures. It is evident that the stiffer the structure, the less chance there is for damping because of ice being ground into small pieces between the pile and the ice edge. To apply this measured damping increase to full-scale structures, one needs to observe the displacement amplitudes carefully.

ICE-INDUCED NEGATIVE DAMPING

With higher velocities during resonance at 2.6 Hz in test 44 the damping measured from the ice force autospectrum peak width indicates a decrease from 19 to 7.8%. This verifies the concept of ice-induced negative damping, which follows theoretically from the negative slope in the ice crushing strength versus loading rate curve.

The measurement of negative slopes from computer plots (Appendix A) did not succeed for all tests. Table 8 contains the data from those tests where negative slopes for average ice forces appeared. The best examples are tests 43 and 49, followed by tests 37 and 39. In Table 7, v is the ice velocity and not the relative velocity between the ice and pile. However, at the end of the load build-up phase as the pile movement stops and crushing starts, the relative velocity is the same as the ice velocity. The damping factor ζ is for a model with a single degree of freedom:

$$\zeta = \frac{\partial F}{\partial v} \cdot \frac{\omega}{2k} \cdot 100 \qquad (8)$$

where ω is pile vibration angular frequency and k is pile stiffness. Equation 8 results directly from the definition of damping force.

In most tests (and evidently in all tests at some velocity intervals) there is a negative slope so steep that it induces aperiodic divergence for ice-induced vibrations. This occurs as crushing starts, after which the pile accelerates rapidly to so high a velocity that the relative velocity between the ice and the pile corresponds to a velocity in the brittle region, with an average zero slope in the ice strength curve. With higher modes the negative damping coefficient is still larger, which explains why the ice action point of the structure can accelerate so rapidly and make the crushing phase short.

Table 8. Negative damping coefficients.

Test number	∂F/∂v *(kNs/cm)*	ζ^* *(%)*	ζ_r *(%)*
37	-1.3	-150	9.8
38	-0.7	- 70	10.5
39	-1.7	-200	10.6
41	-1.4	-160	10.6
42	-1.4	-160	10.4
43	-3.6	-130	9.2
44	-0.7	- 30	7.8
49	-0.45	- 50	10.3

*ζ = momentary damping factor, ζ_r = equivalent damping factor for a full vibration cycle.

The last column in Table 7 gives the damping ratios at 8.5 Hz (or 2.6 Hz in tests 43 and 44) during continuous crushing. These ratios are measured from the widths of ice force autospectra. The ratio ζ_r is the equivalent viscous damping, which averages the real nonlinear damping during the whole vibration cycle. Thus, even though ice-induced negative damping is supercritical, it appears only for a part of the vibration cycle; the result is that damping ratios remained practically unchanged at 8.5 Hz and decreased from 19.0 to 7.8% at 2.6 Hz. The overall effect of ice-induced negative damping is more than these figures indicate because the ice also induces positive damping. This contribution should be added if the total negative damping effect is desired.

LIMIT CYCLES

Measurement data plots show that the ice force repeats itself continuously in consistent patterns. The vibrations of the pile have reached a steady state limit cycle. This means that autonomous self-excited vibrations have developed. The reason for the rise of vibrations is the high negative ice-induced damping, which causes dynamic instability in the small (the growth of infinitesimal disturbances into distinguishable increasing dynamic response). However, stability in the large exists because vibrations and ice forces fluctuations stabilize at a steady level.

The limit cycles can be predicted analytically by starting with the averaged ice crushing strength curves and taking into account the dynamic response of the structure, yielding similar response and ice force patterns to those that were measured. Figure 13 is the numerically integrated ice force history for test 40. Even though there are differences, the force pattern and frequency correspond to the measured response (Fig. 8a). Analytically predicted stable and unstable modes were verified by the measurements. The 8.5-Hz mode of the test pile was very unstable, and the measurements exhibited continuous vibrations. The

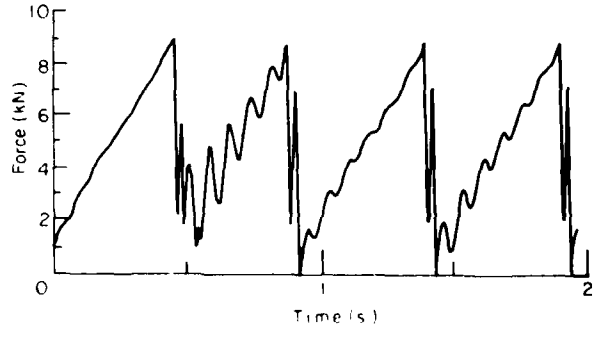

Figure 13. Ice force plot generated by numerical integration starting from the ice crushing strength curve (test 40, v = 10 mm/s).

second mode (60 Hz) was also unstable, indicating the initiation of this mode at high ice velocities. In two tests the 2.6-Hz mode was stable; there did not appear to be any resonant vibrations in this frequency. Vibrations at 2.2–2.8 Hz are due to resonance with the carriage. These comparisons with theory and measurements are additional evidence that ice-induced negative damping is the reason for ice-induced structural vibrations and that both the ice and the structure affect the observed ice forces.

BUCKLING LOAD

Tests 50 and 51 give a check on buckling load theories. Even though no analytical or Finite Element Method (FEM) solutions are presented for the exact geometry of a circular pile in an infinite ice field, the FEM model by Sodhi[20] is close enough to the problem in question. For compressive stresses against the pile, frictionless boundary conditions and a modulus of elasticity of 3 GPa yield buckling loads of 27 kN or greater. The measured buckling loads were 3.2 and 3.7 kN with 102- and 178-mm pile diameters, respectively.

Ice index strength tests were still being developed, and therefore the measured values for the modulus of elasticity are not very accurate. Instead, the modulus of elasticity can be calculated from the measured buckling load. The curves of Sodhi shows a characteristic length of about 350 mm, which corresponds to a modulus of elasticity of 0.22 GPa.

Buckling developed in 2–3 seconds. Thus, the loading rate is high enough so that viscoelastic yielding can not be the sole reason for the difference. The linear theory itself must be at least part of the reason. Kerr[22] has proved (but not solved the real case) that the bifurcation point in the equilibrium path of the plate on the elastic foundation under in-plane loads is unstable. This means that imperfection sensitivity can significantly reduce buckling loads. Meaningful comparisons between the measurements and the theory will become possible after the nonlinear buckling problem is solved.

In both buckling cases, the ice failed by buckling only when the velocities were below 5 mm/s; above this velocity only crushing failure occurred. For a given ice sheet the test with a small pile did not produce any buckling, e.g. test 49. This indicates that buckling and crushing loads were almost identical at the low velocities in tests 50 and 51. A slight change in conditions was enough to change the mode of failure from buckling to crushing. With increasing velocity the effective modulus of elasticity of ice increased while viscoelastic effects were decreasing; the foundation modulus also increased due to increasing hydrodynamic support effects.

These measurements and the analysis of the results suggest that for wide full-scale structures with slowly moving ice, buckling can occur before crushing. This could be important for design ice forces. However, as the nonlinear buckling model is missing, it is not possible to locate the boundary between crushing and buckling.

CONCLUSIONS

Model tests conducted at the CRREL Ice Engineering Facility during December 1979 and January 1980 provided valuable data for understanding dynamic ice-structure interactions during crushing. The test arrangements allow scale-model studies for most bottom-founded offshore structures. In this study, only constant-thickness ice was used, but modeling is possible for rafted ice and pressure ridges as well.

In these test arrangements the weakest link is the inadequate stiffness of the ice-pushing system. The dynamic response of the ice-pushing system still interfered at low velocities, even though the whole velocity range from ductile to brittle could be measured.

Experiences with urea-doped ice confirm that sea-ice grain structures and crushing failure types are similar. The crushing strength and the modulus of elasticity have the same ratio. Hence, scale model measurements can be made that are accurate and simple to interpret.

The general behavior of the ice force and pile vibrations was such that at low velocities, a sawtooth ice force and pile displacement pattern developed. With increasing velocity the lowest natural mode of the pile was excited; it dominated the response until the velocity became too high for the first mode to follow. Then either higher frequency ice forces appeared or the second mode of the structure became dominant. The shift from the sawtooth pattern to the natural modes of the structure occurred in each test.

Maximum ice forces usually occurred at low velocities in the range of loading rate from ductile to brittle. The maximum and average ice force, as well as the standard deviation, tended to be lower with increasing velocity, although the random peaks of the ice force at high velocities may equal the peaks at low velocities. There is more randomness with freshwater ice than with urea-doped ice. For design purposes a good estimate of the maximum ice force is the average plus three times the standard deviation.

These tests were the first to measure the effect of the ratio of pile diameter to ice thickness on the effective ice pressure under continuous dynamic crushing. The results indicate that a similar dependence of ice force on aspect ratio under static conditions holds with sufficient accuracy. It appeared that in urea ice the proportion of the ice layer with a horizontal c-axis more strongly affects the crushing strength than the bending strength.

The frequency of the observed ice force is directly proportional to the ice velocity and inversely proportional to the ice force fluctuation range. The natural frequencies of the pile dominate the frequency response in such a way that the crushing frequency stays close to the natural frequency, and instead of the frequency increasing with velocity, it causes the ice force range to increase with velocity.

The test results support the theory that the crushing frequency can be calculated from the product of the structural stiffness at the ice action point and the ice velocity divided by the observed ice force. The dominating feature of natural frequencies has to be taken into account and the effective structural stiffness observed if applicable. Thus, the whole range of observed frequencies can be described by a simple equation.

Theoretical predictions according to the theory of ice-induced, self-excited vibrations yield similar results. Another theory, which says that the crushing frequency can be determined by the property of ice to fail into floes of a certain size, did not agree with the test data. Peyton's suggestion that ice has a characteristic failure frequency was disproved. With changing velocity the crushing frequency usually changes; it remains constant only at the expense of the ice force or displacement amplitudes and is the result of a dominant natural mode of the structure.

The acceleration data reveal that during crushing, high frequency components were present and gave the highest accelerations. After crushing, the structure settles down to first or second mode vibrations. While the ice edge sticks to the pile during load build-up, it provides additional support, which increases the natural frequencies. Integrated velocities verify that the pile deflection rate is so high that the ductile loading rate can exist during the whole velocity range, despite the fact that the ice velocity alone would result in brittle loading rates.

Damping measurements indicated that ice crushing, friction and the grinding of ice into rubble against the pile created considerable positive damping, more than six times that of the pile alone. However, the negative damping effects of the ice were so high that aperiodic divergences occurred at the beginning of crushing. As this was only during a part of the vibration cycle, the average damping, or the equivalent viscous damping, was still positive.

The origin of ice-induced vibrations was verified. The negative damping caused dynamic instability in the small, but as the overall damping was positive, the steady state vibrations stabilized and the pile reached its limit cycles. Ice force histories for structures similar to those measured can be calculated using the ice-crushing strength vs loading rate curves and adjusting for the dynamic response. This gives a basis for better design against dynamic ice forces.

LITERATURE CITED

1. **Blenkarn, K.A.** (1970) Measurement and analysis of ice forces on Cook Inlet structures. Offshore Technology Conference, Dallas, Texas.
2. **Eranti, E.** (1979) Indentation experiments with natural ice plates. Publication 21, Laboratory of Structural Technology, Helsinki University of Technology, Helsinki, Finland.
3. **Frederking, R. and L. Gold** (1971) Ice forces on an isolated offshore pile. *Proceedings of the First International Conference on Port and Ocean Engineering Under Arctic Conditions.* Technical University of Norway, Trondheim.
4. **Frederking, R. and L. Gold** (1975) Experimental study of edge loading of ice plates. *Canadian Geotechnical Journal,* **12**(4): 456-464.
5. **Haynes, F.D., D.E. Nevel and D.R. Farrell** (1975) Ice force measurements on the Pembina River, Alberta. CRREL Technical Report 269.
6. **Hirayama, K., J. Schwartz and H.C. Wu** (1973) Model technique for the investigation of ice forces on structures. *Proceedings of the Second International Conference on Port and Ocean Engineering Under Arctic Conditions.* University of Iceland, Reykjavik.
7. **Michel, B. and N. Toussaint** (1976) Mechanism and theory of indentation of ice plates. Symposium on Applied Glaciology, Cambridge.
8. **Montgomery, C.J., R. Gerard and A.W. Lipsett** (1980) Dynamic response of bridge piers to ice forces. *Canadian Journal of Civil Engineering,* **7**: 345-356.
9. **Nevel, D.E., R.E. Perham and G.B. Hogue** (1977) Ice forces on vertical piles. CRREL Report 77-10.
10. **Wu, H.C., K.J. Chang and J. Schwartz** (1976) Fracture in the compression of columnar grained ice. *Engineering Fracture Mechanics,* **8**: 365-372.
11. **Määttänen, M.** (1979) Laboratory tests for dynamic ice-structure interaction. *Proceedings of the Fifth International Conference on Port and Ocean Engineering Under Arctic Conditions.* Norwegian Institute of Technology, Trondheim.

12. **Määttänen, M.** (1975) Experiences of ice forces against a steel lighthouse mounted on the seabed, and proposed constructional refinements. *Proceedings of the Third International Conference on Port and Ocean Engineering Under Arctic Conditions.* University of Alaska, Fairbanks.
13. **Peyton, H.R.** (1966) Sea ice forces–Conference on ice pressure against structures. National Research Council Technical Memorandum No. 92, Laval University, Quebec.
14. **Peyton, H.R.** (1968) Ice and marine structures, Reprint from *Ocean Industry,* Parts 1, 2 and 3, March, September and December.
15. **Määttänen, M.** (1978) On conditions for the rise of self-excited ice induced autonomous oscillations in slender marine pile structures. Finnish-Swedish Winter Navigation Board, Research Report No. 25, Finnish Board of Navigation, Helsinki.
16. **Neill, C.** (1976) Dynamic ice forces on piers and piles–An assessment of design guidelines in the light of recent research. *Canadian Journal of Civil Engineering,* 3: 305-341.
17. **Reddy, D.V., P.S. Cheema and A.S.J. Swamidas** (1975) Ice force response spectrum modal analysis of offshore towers. *Proceedings of the Third International Conference on Port and Ocean Engineering Under Arctic Conditions.* University of Alaska, Fairbanks.
18. **Timco, G.W.** (1980) The mechanical properties of saline-doped and carbamide (urea)-doped model ice. *Cold Regions Science and Technology,* **3**: 45-56.
19. **Neill, C., J. Saunders and M. Schultz** (1971) Measurements of ice forces on bridge piers, 1970 and 1971. Research Council of Alberta, Edmonton, Alberta.
20. **Sodhi, D.** (1979) Buckling analysis of wedge-shaped floating ice sheets. *Proceedings of the Fifth International Conference on Port and Ocean Engineering Under Arctic Conditions.* Norwegian Institute of Technology, Trondheim.
21. **Working Group of the IAHR Section on Ice Problems** (1980) Standardization of testing methods for ice properties. *Journal of Hydraulic Research,* **18**(2): 153-165.
22. **Kerr, A.** (1980) On the buckling force of floating ice plates. *Proceedings, IUTAM Physics and Mechanics of Ice Symposium* (P. Tryde, Ed.), Copenhagen. New York: Springer Verlag.

APPENDIX A: CORRECTED ICE FORCE VS TIME FOR TESTS 39 AND 44.

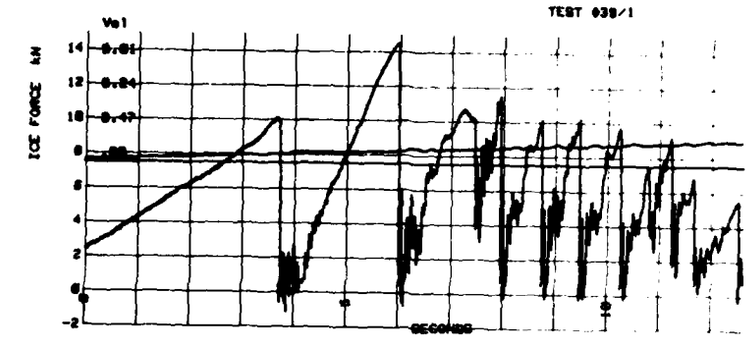

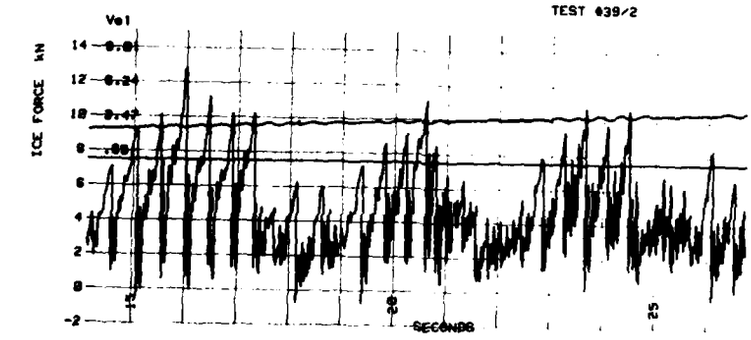

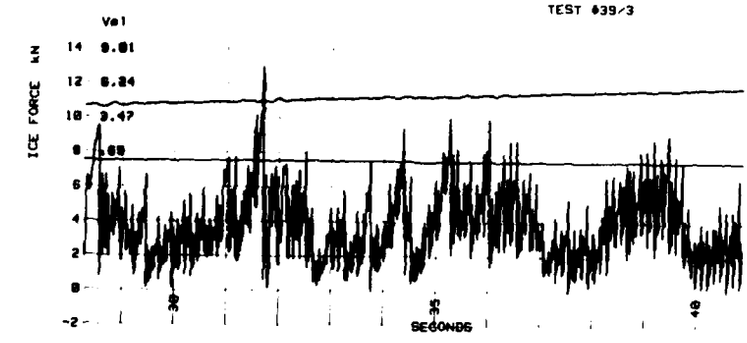

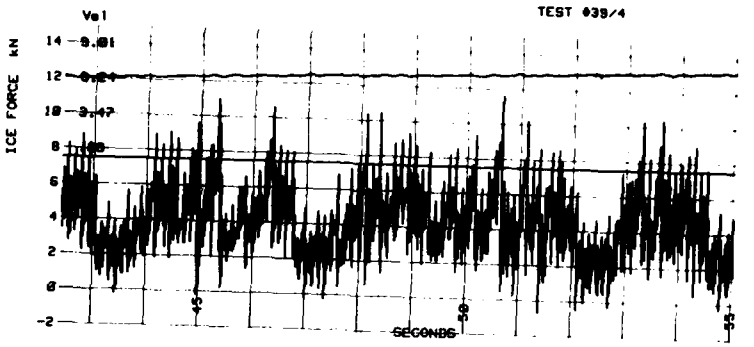
Vel
TEST #39/4
ICE FORCE kN
14 9.01
12 6.24
10 3.47
8
6
4
2
0
-2
45
50
SECONDS

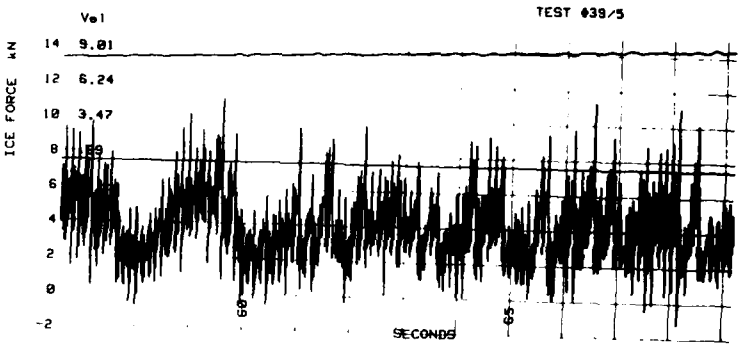
Vel
TEST #39/5
ICE FORCE kN
14 9.01
12 6.24
10 3.47
8
6
4
2
0
-2
60
65
SECONDS

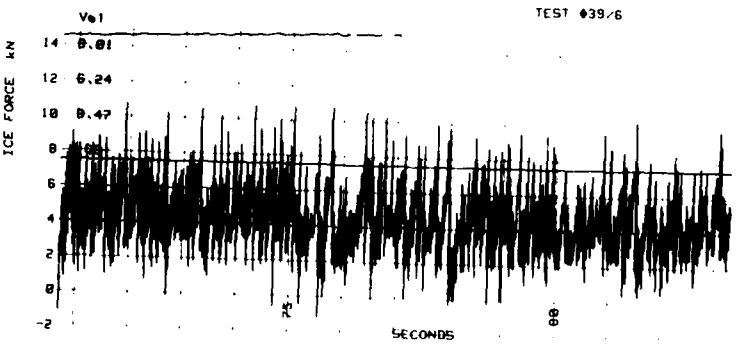
Vel
TEST #39/6
ICE FORCE kN
14 9.01
12 6.24
10 3.47
8
6
4
2
0
-2
75
80
SECONDS

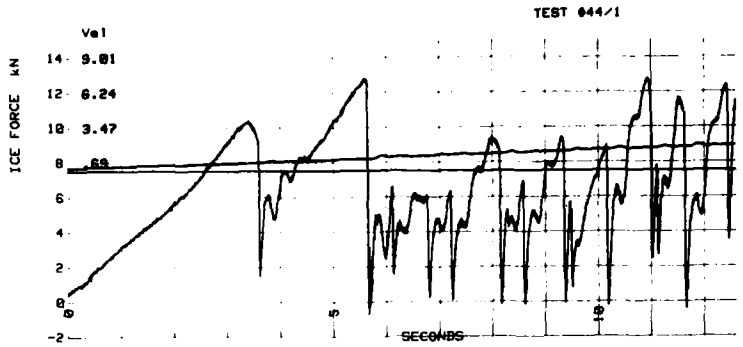
TEST 044/1
Vel
14 9.81
12 6.24
10 3.47
8 .69
6
4
2
0
-2
ICE FORCE kN
0
5
10
SECONDS

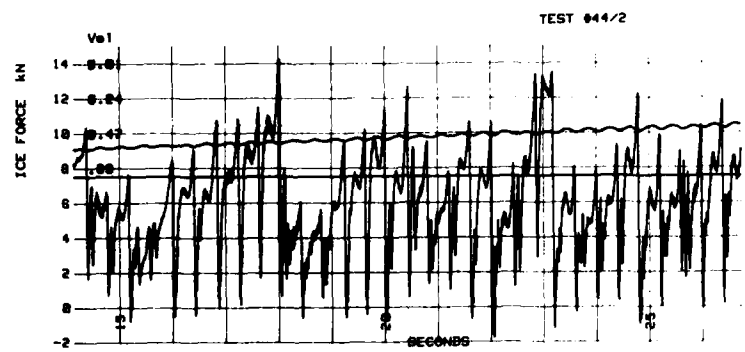
TEST 044/2
Vel
14
12
10
8
6
4
2
0
-2
ICE FORCE kN
0
5
10
SECONDS

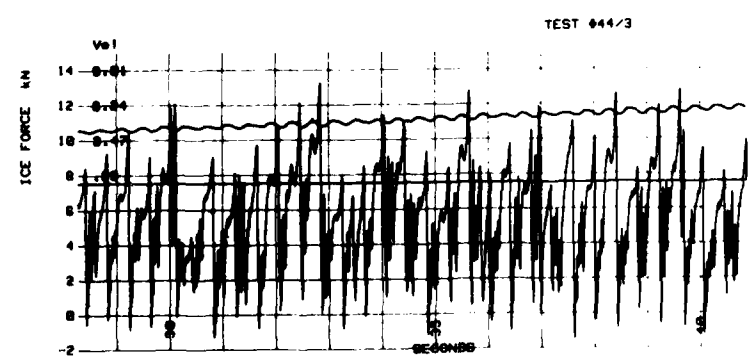
TEST 044/3
Vel
14
12
10
8
6
4
2
0
-2
ICE FORCE kN
0
5
10
SECONDS

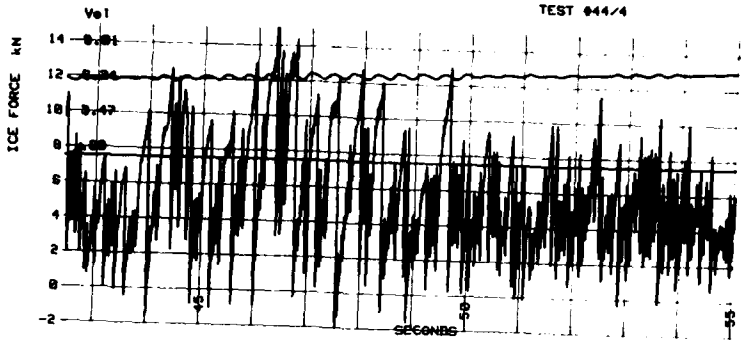
Vel
TEST 044/4
ICE FORCE kN
14
12
10
8
6
4
2
0
-2
45
50
55
SECONDS

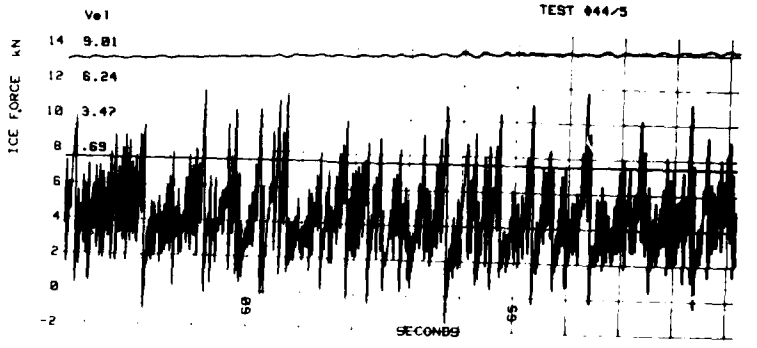
Vel
TEST 044/5
ICE FORCE kN
14 9.81
12 6.24
10 3.47
8 .69
6
4
2
0
-2
60
65
SECONDS

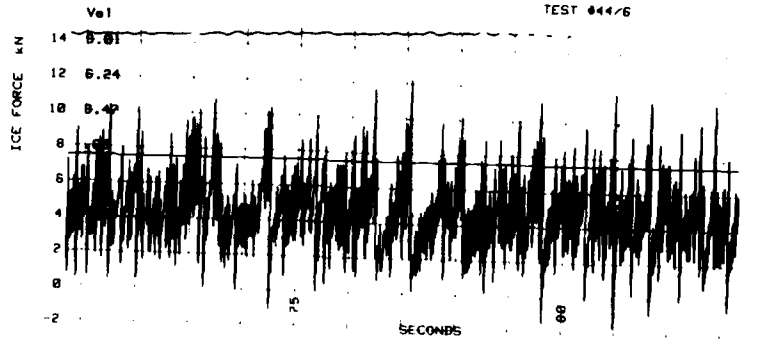
Vel
TEST 044/6
ICE FORCE kN
14 9.81
12 6.24
10 3.47
8
6
4
2
0
-2
75
80
SECONDS

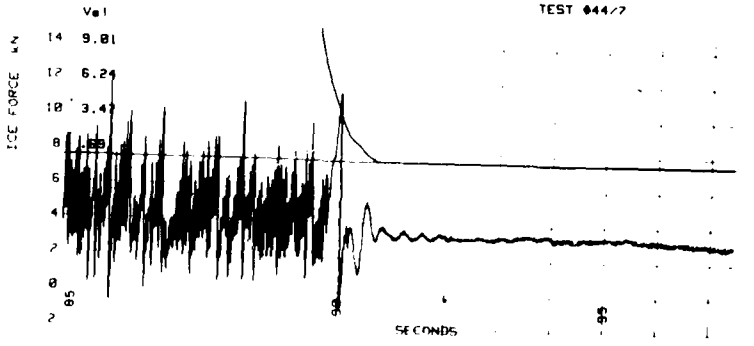
Vel
TEST 044/7
ICE FORCE kN
14 9.81
12 6.24
10 3.47
8
6
4
2
0
-2
85
90
95
SECONDS

APPENDIX B: ICE FORCE VS VELOCITY WITH 3.15-SECOND SAMPLING PERIOD

(x = maximum ice force, * = average ice force, 0 = standard deviation).

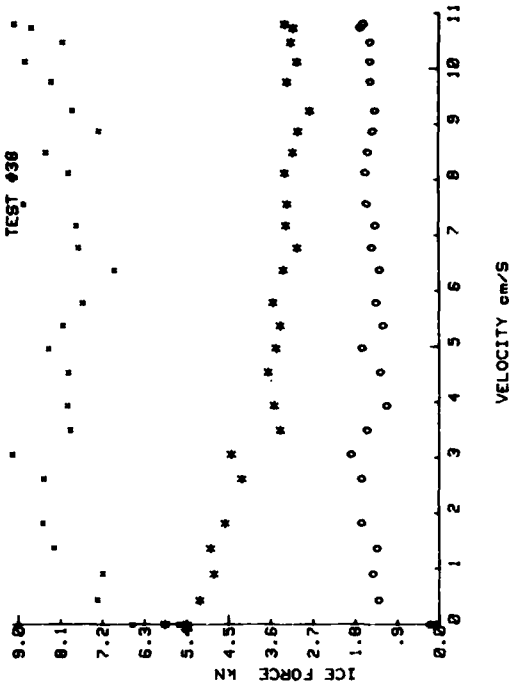

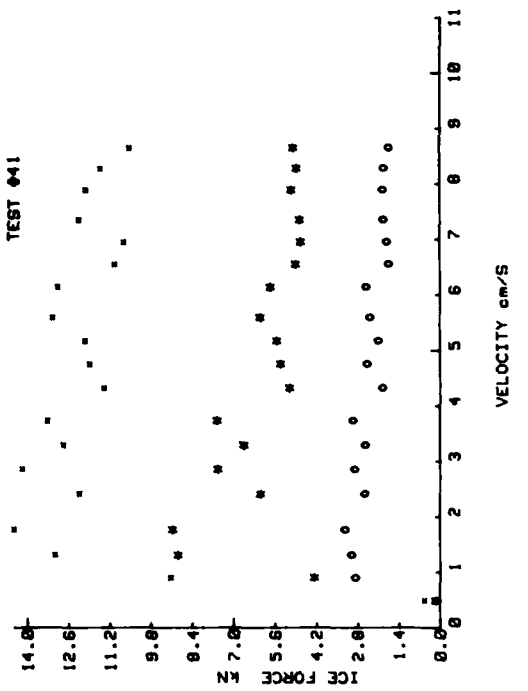

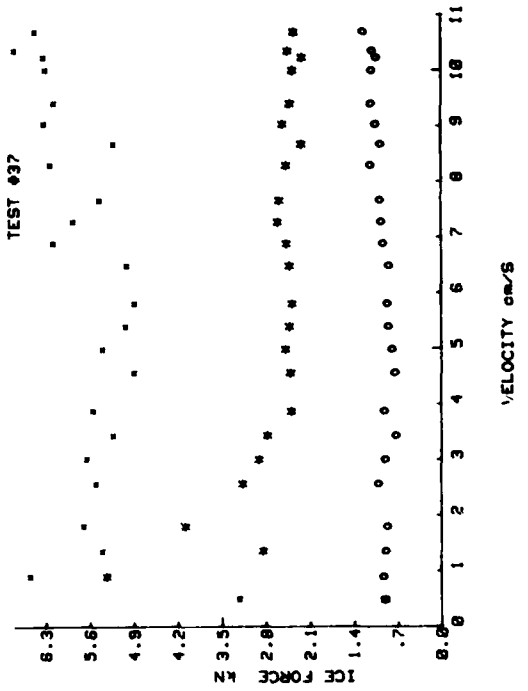

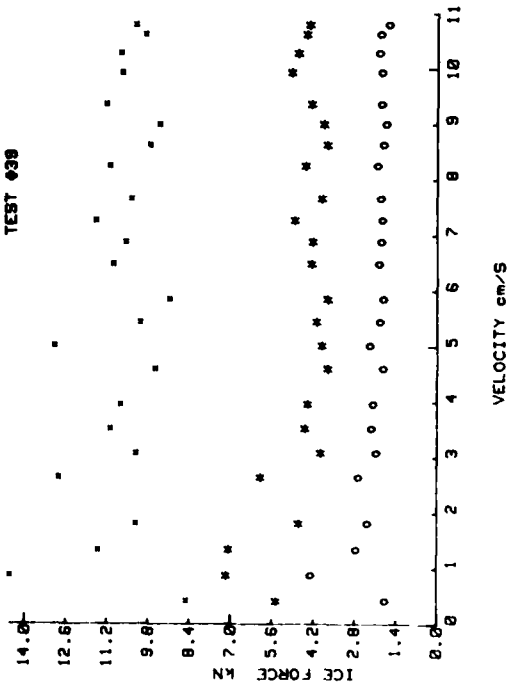

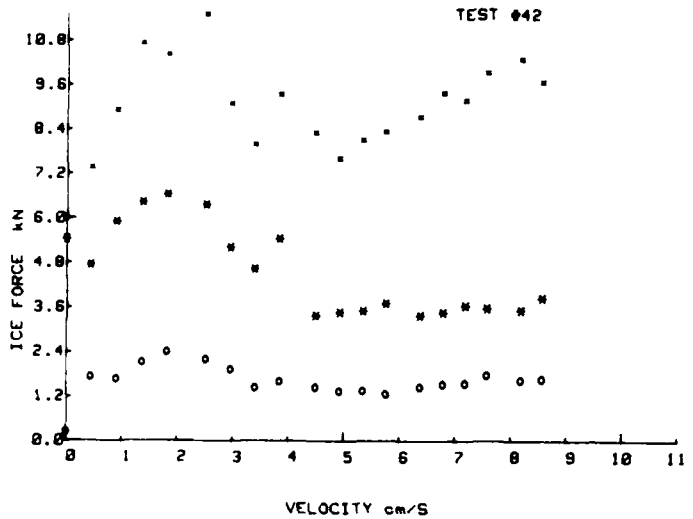
TEST #42
ICE FORCE kN
VELOCITY cm/S

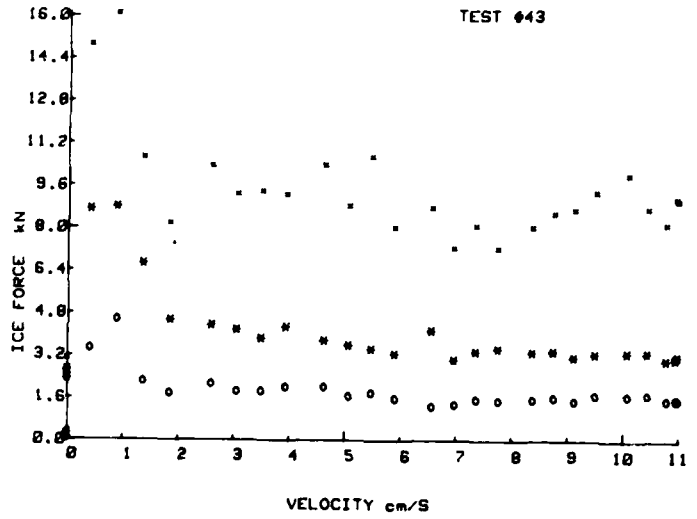
TEST #43
ICE FORCE kN
VELOCITY cm/S

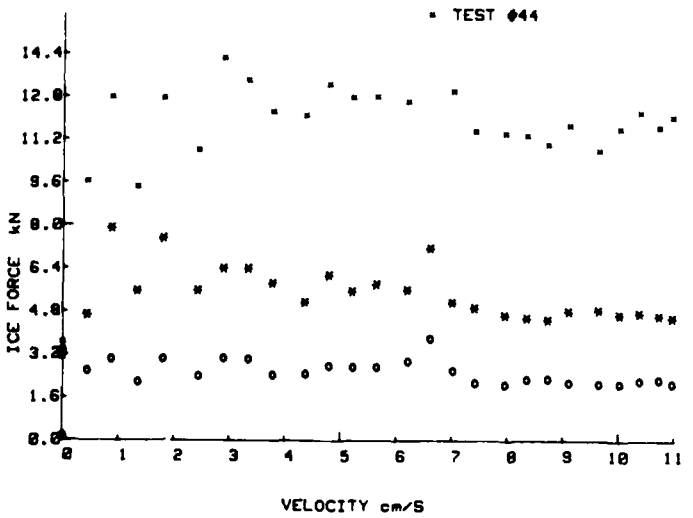
TEST #44
ICE FORCE kN
VELOCITY cm/S

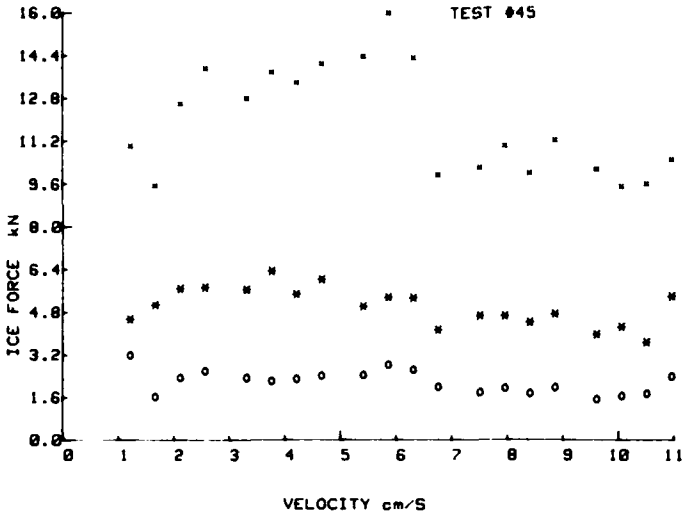
TEST #45
ICE FORCE kN
VELOCITY cm/S

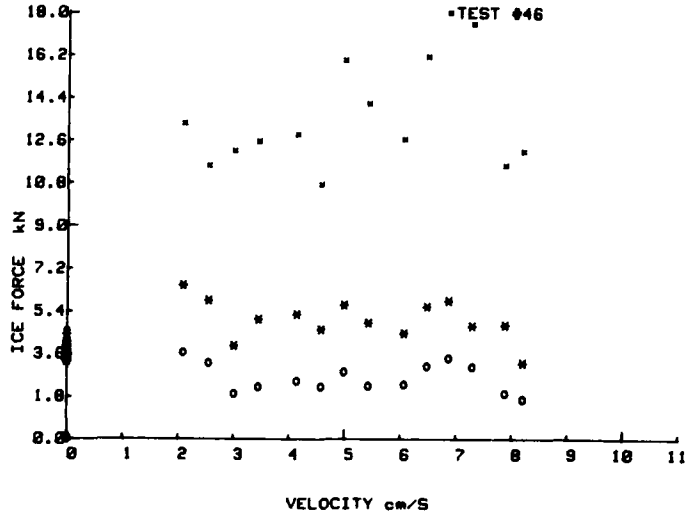
TEST #46
ICE FORCE kN
VELOCITY cm/S

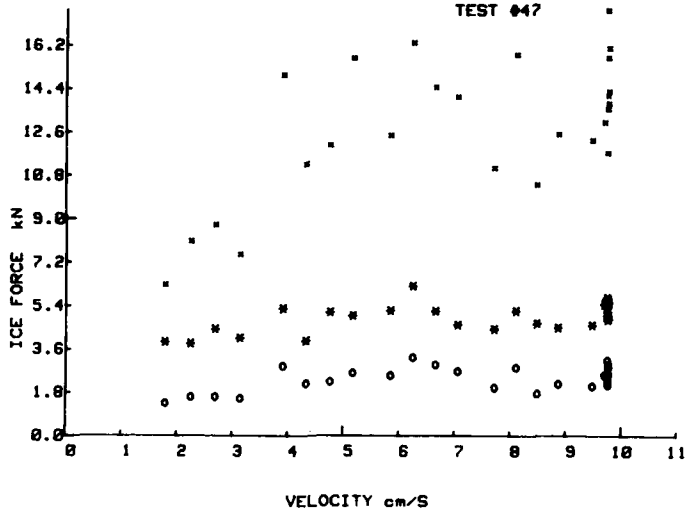
TEST #47
ICE FORCE kN
VELOCITY cm/S

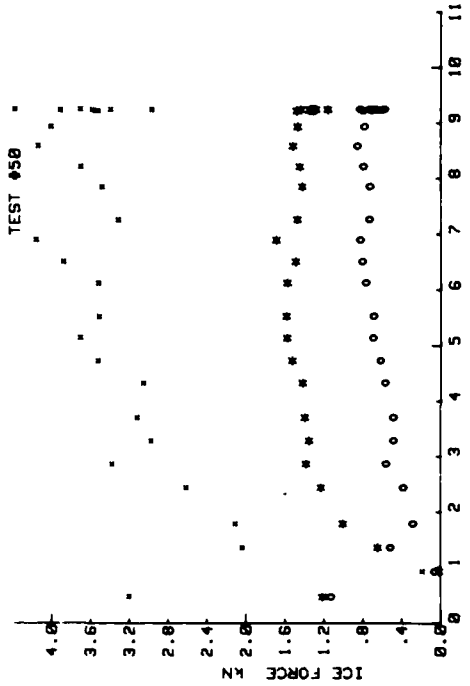
TEST #50
ICE FORCE kN
VELOCITY cm/S

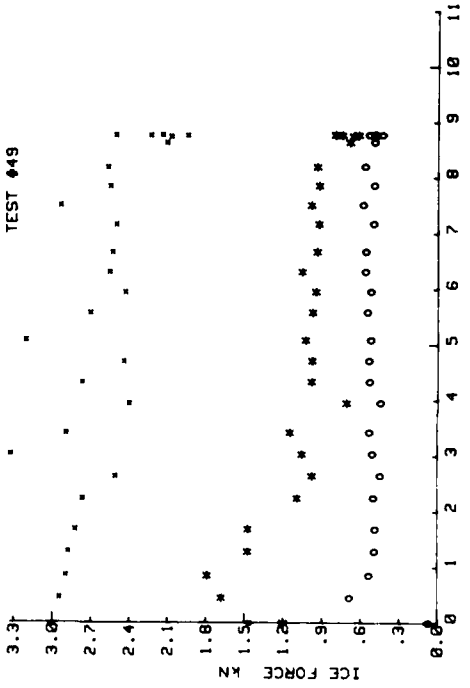
TEST #49
ICE FORCE kN
VELOCITY cm/S

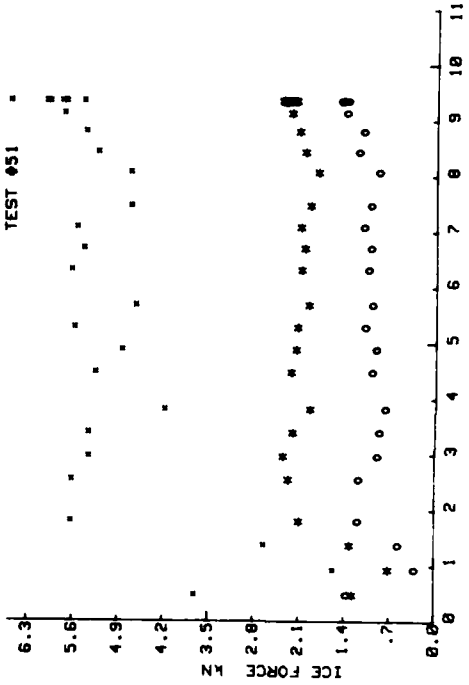
TEST #51
ICE FORCE kN
VELOCITY cm/S

APPENDIX C: UNCORRECTED ICE FORCE, VELOCITY AND ACCELERATION VS TIME FOR TESTS 39 AND 44.

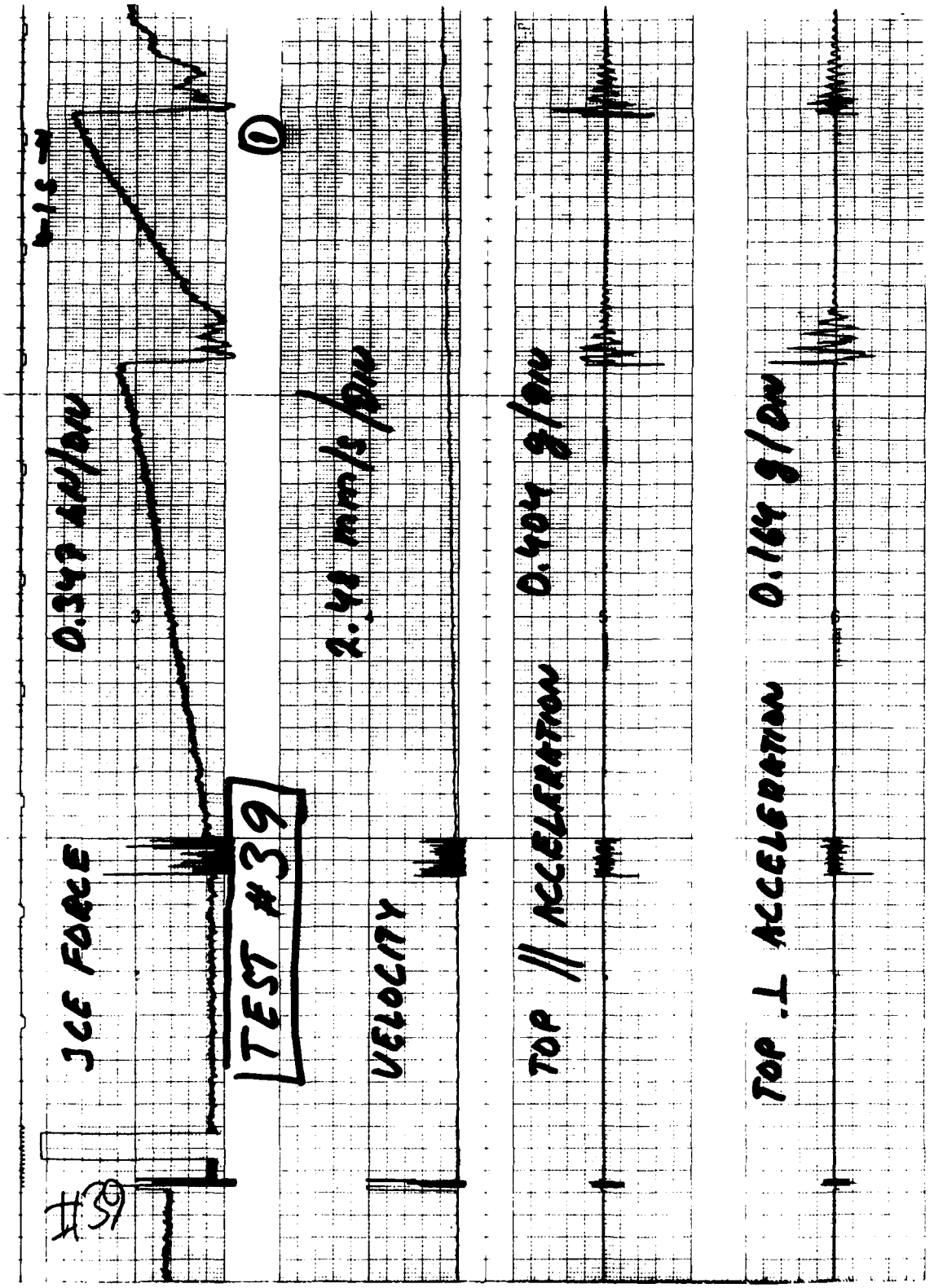

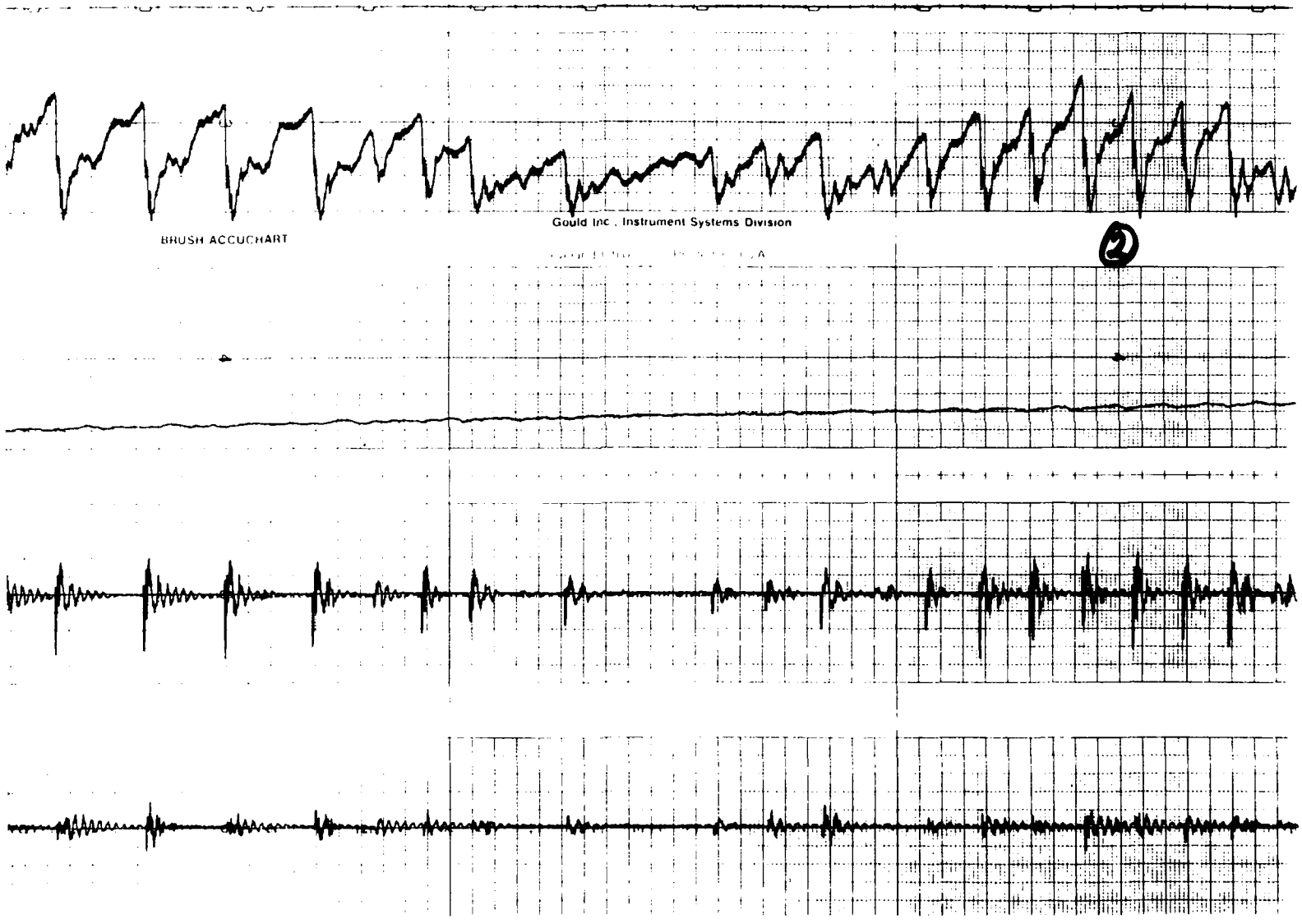
BRUSH ACCUCHART
Gould Inc. Instrument Systems Division
2

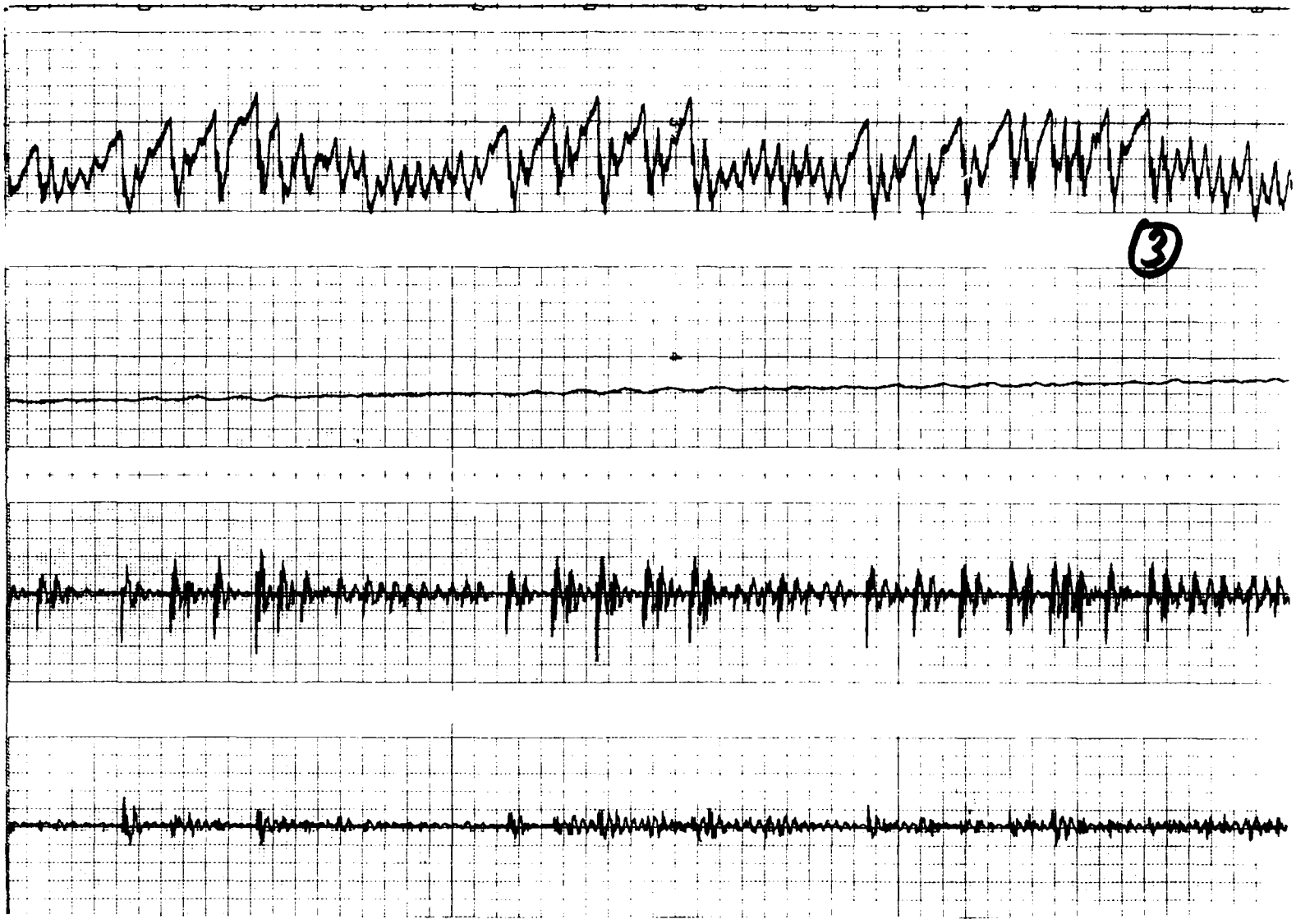
3

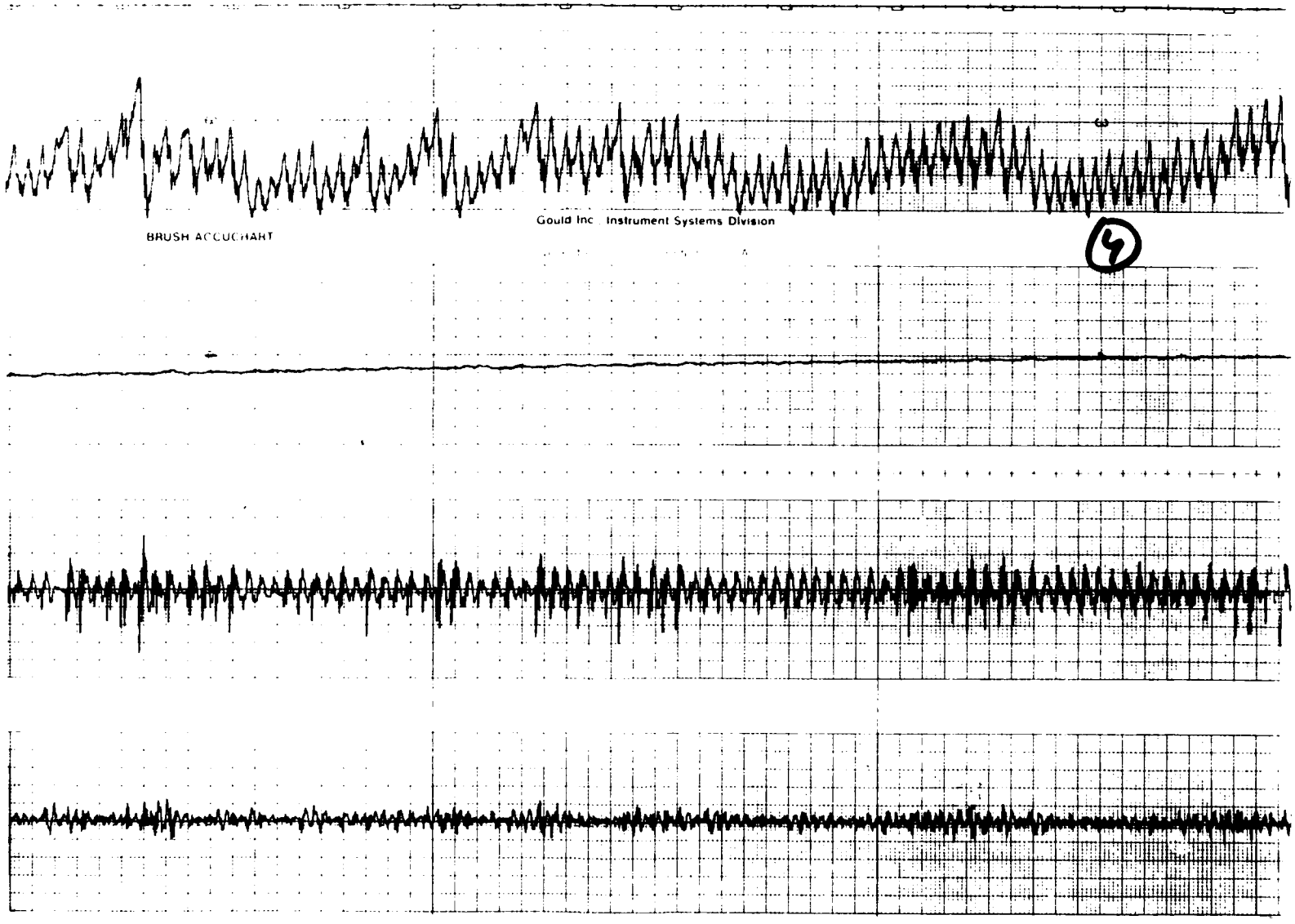
BRUSH ACCUCHART
Gould Inc. Instrument Systems Division
(4)

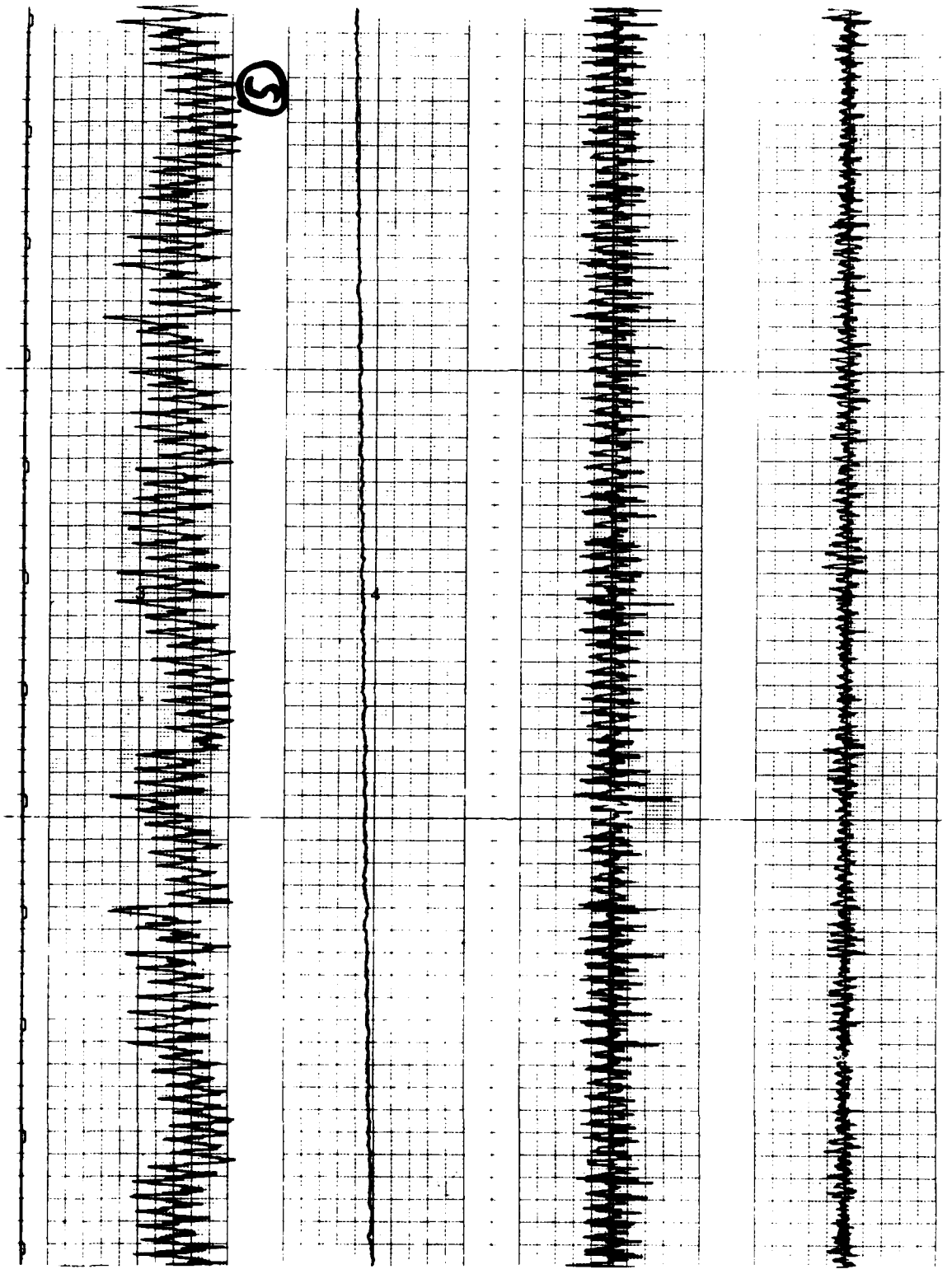

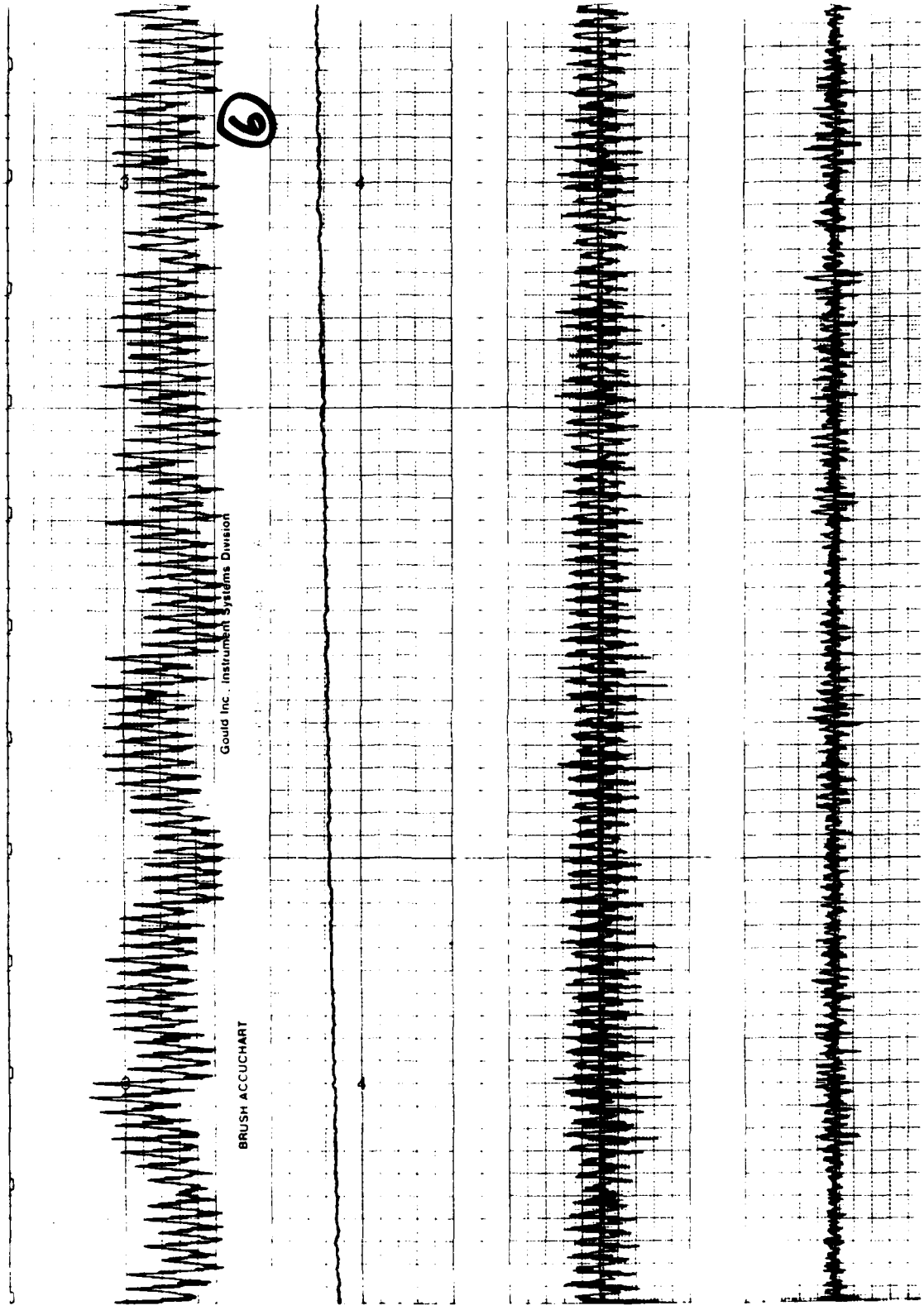
6
Gould Inc., Instrument Systems Division
BRUSH ACCUCHART

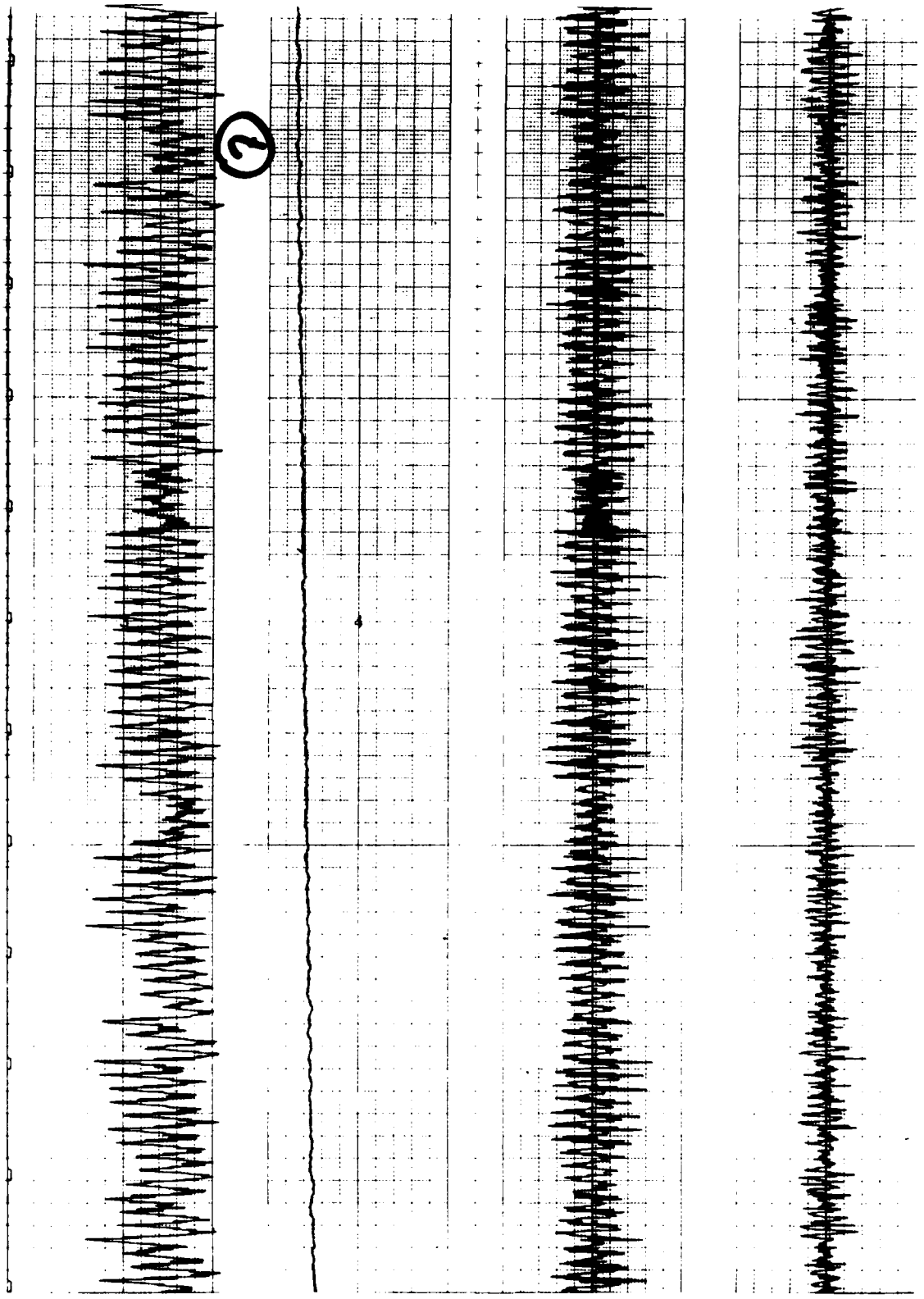

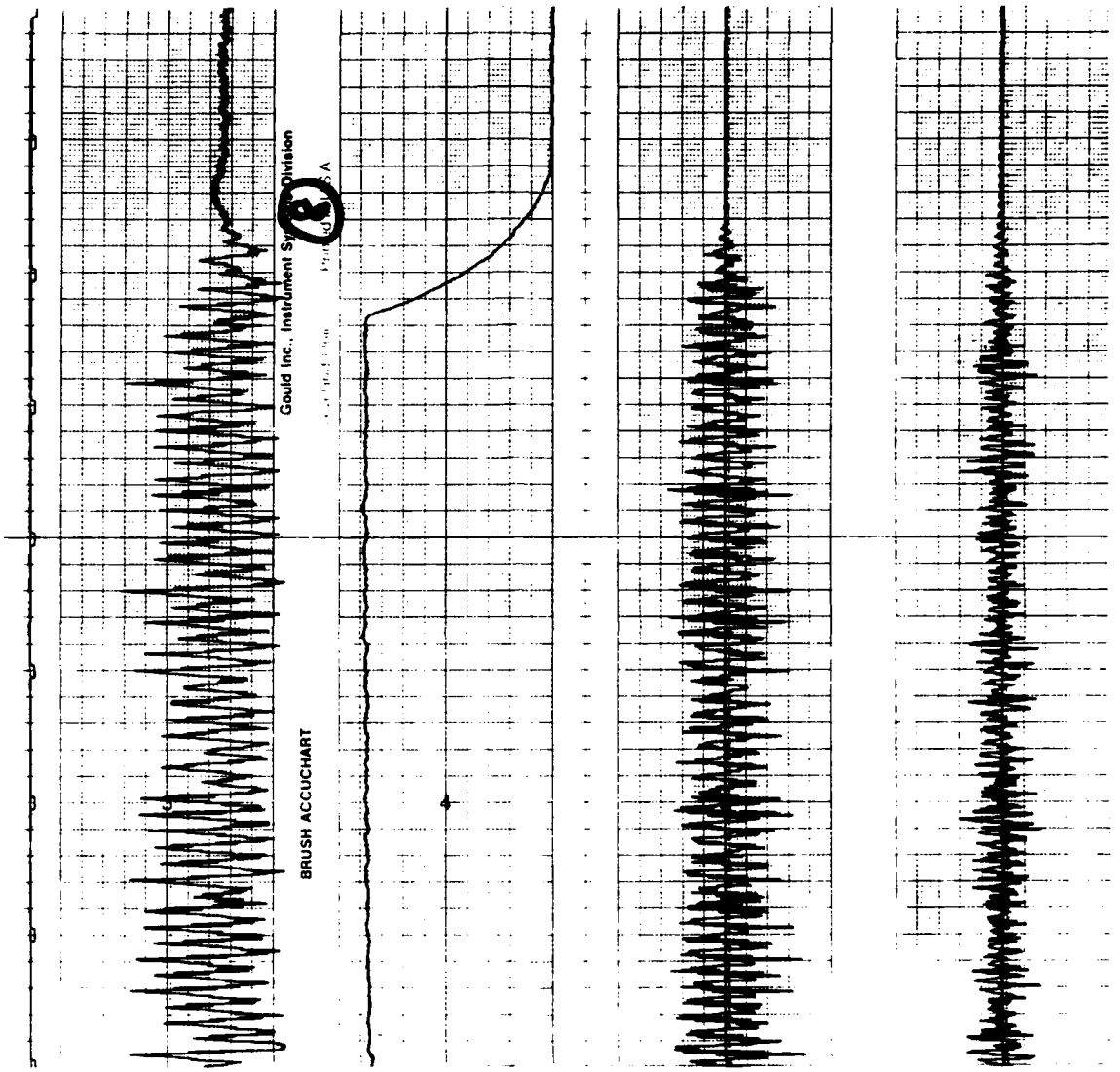
Gould Inc., Instrument Systems Division
BRUSH ACCUCHART

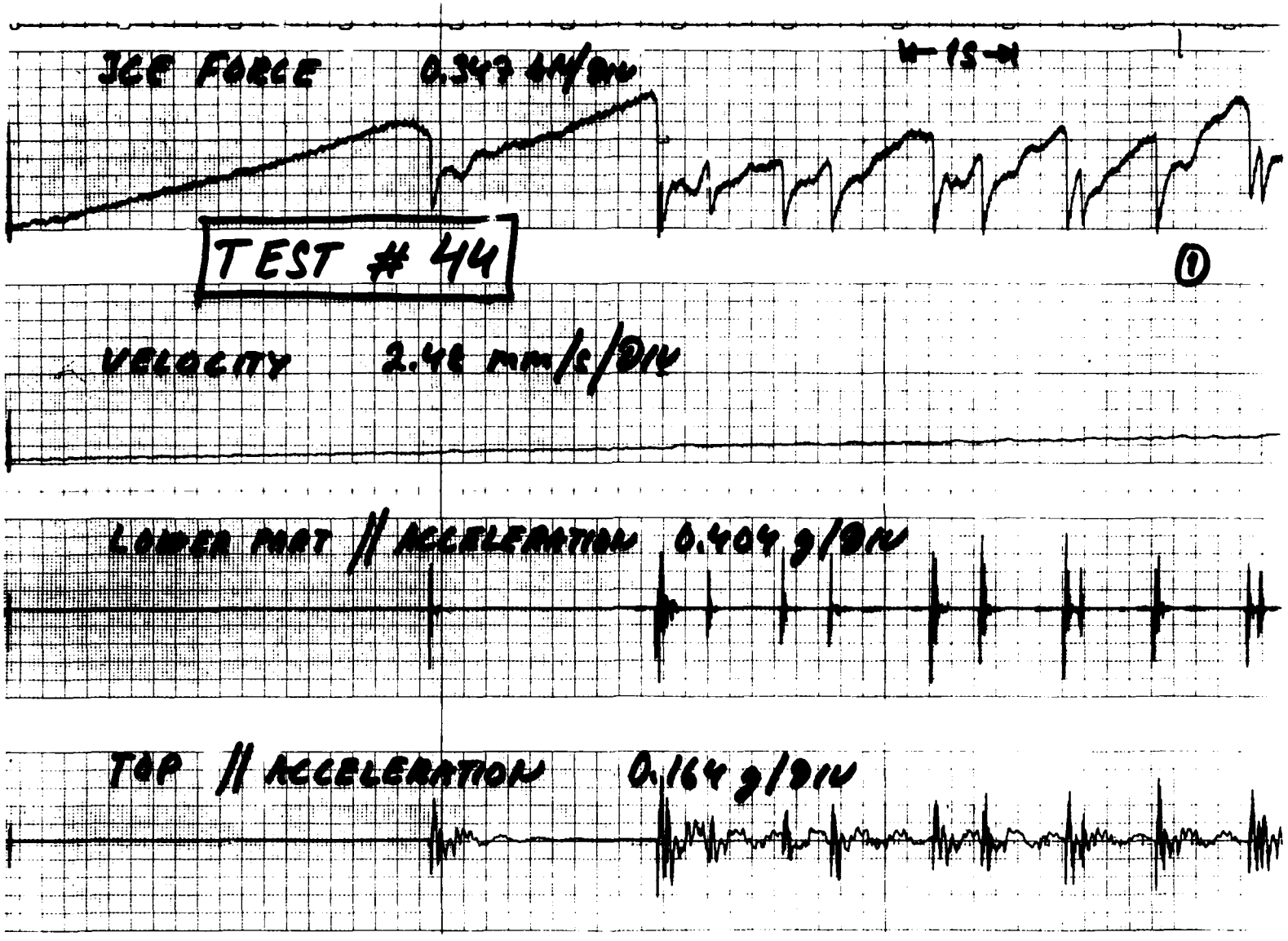
ICE FORCE 0.347 kN/Div
1 SEC
TEST # 44
1
VELOCITY 2.48 mm/s/Div
LOWER MAT // ACCELERATION 0.404 g/Div
TOP // ACCELERATION 0.164 g/Div

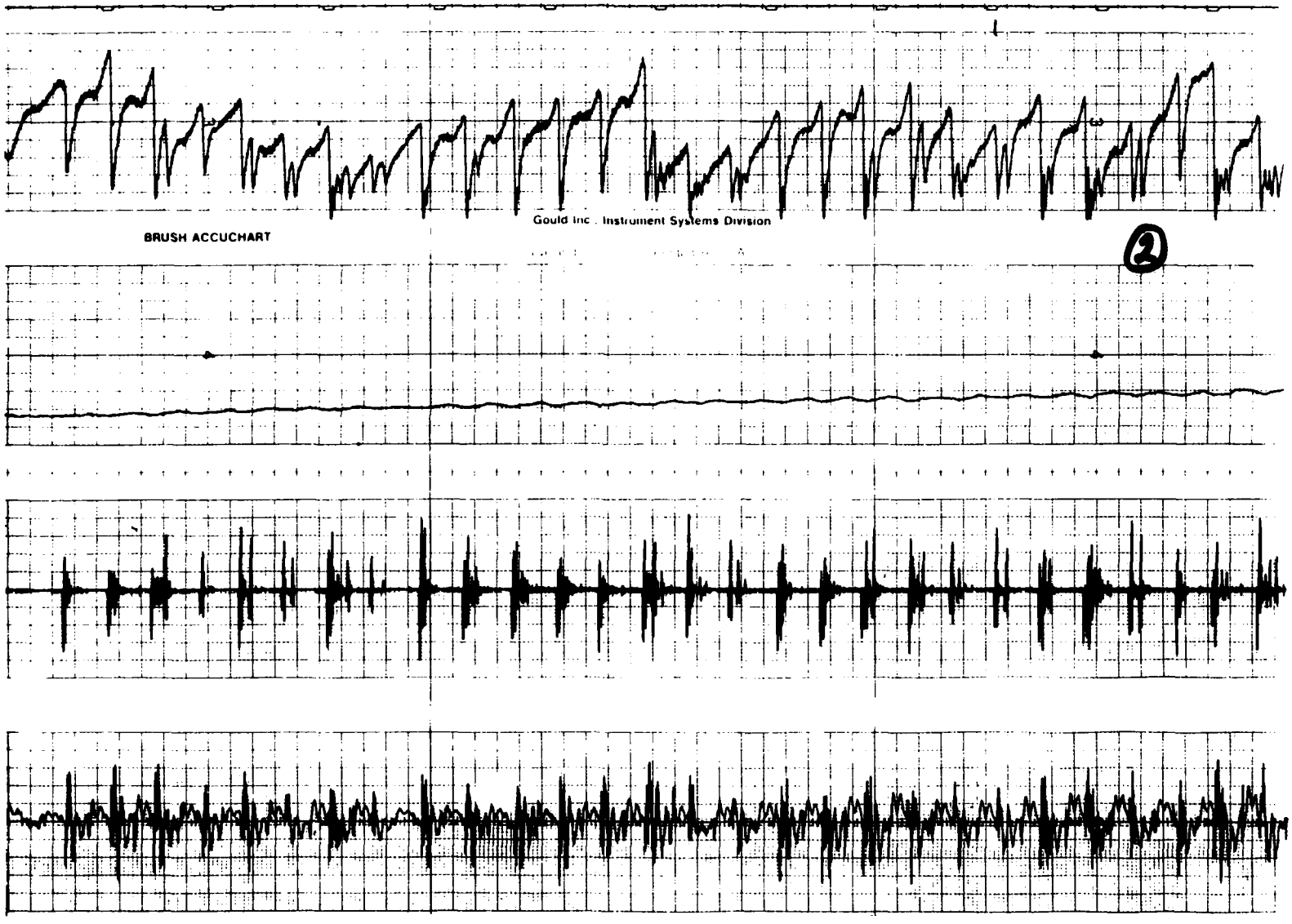
Gould Inc. Instrument Systems Division
BRUSH ACCUCHART
2

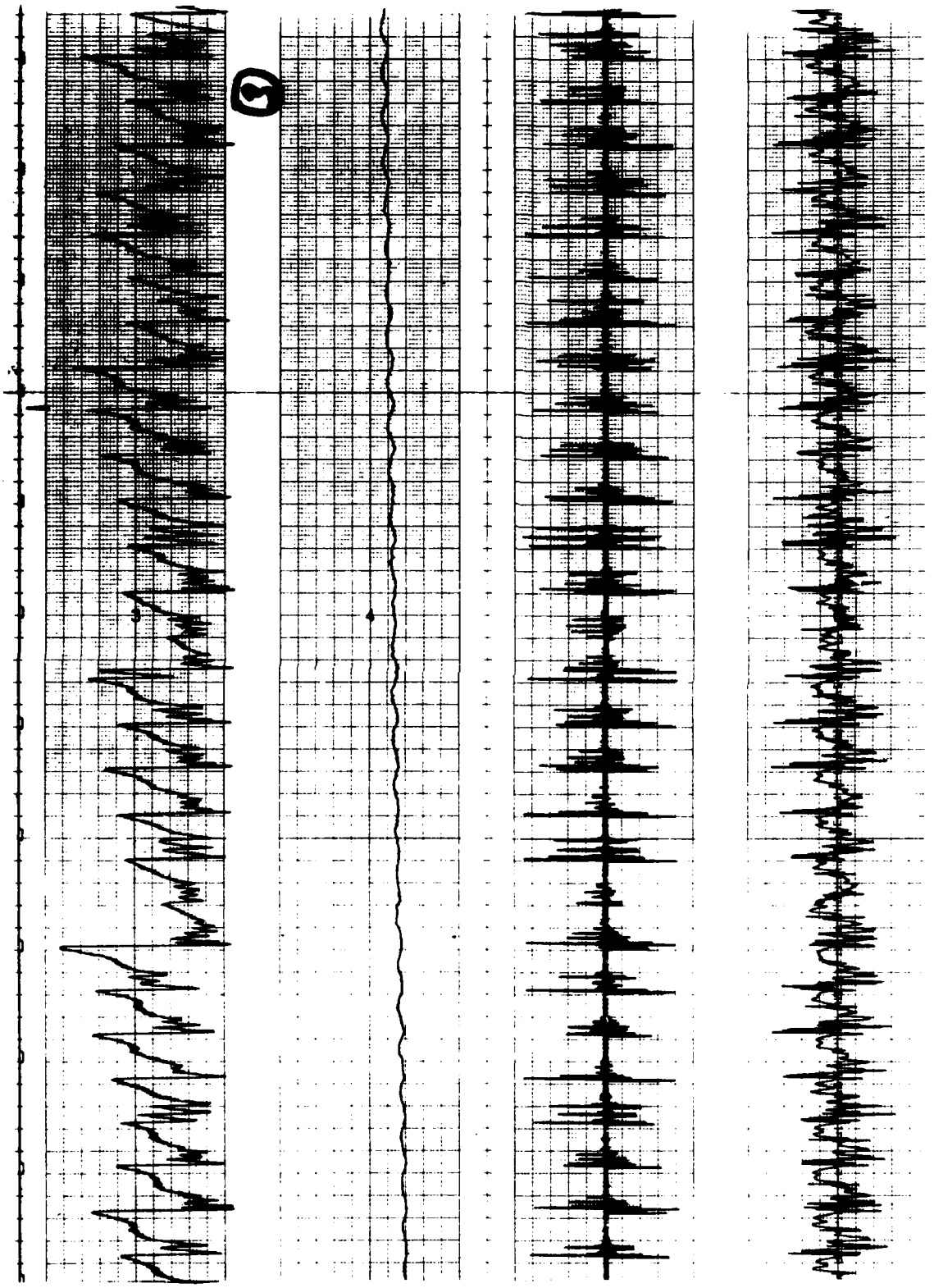

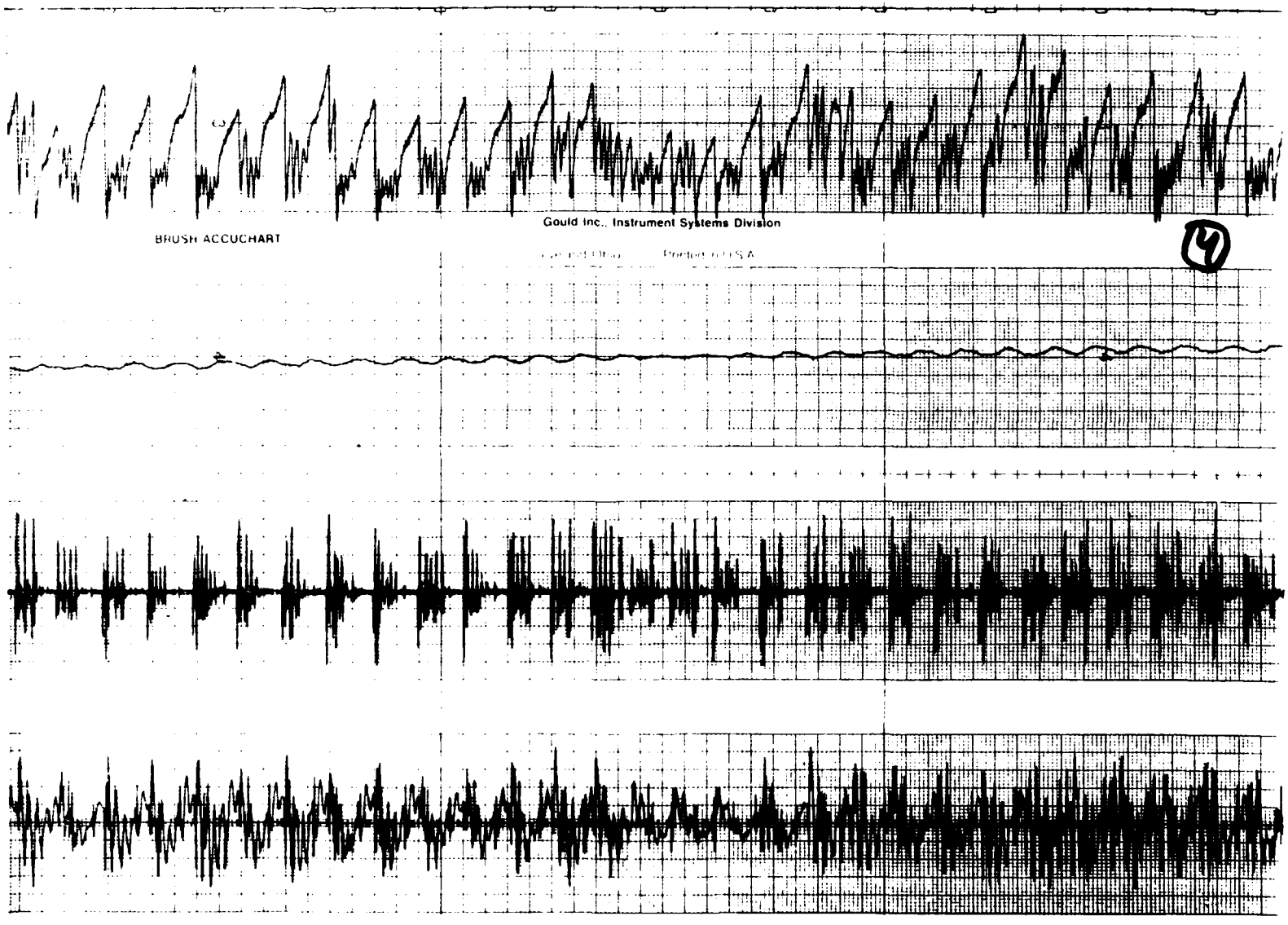
BRUSH ACCUCHART
Gould Inc., Instrument Systems Division
4

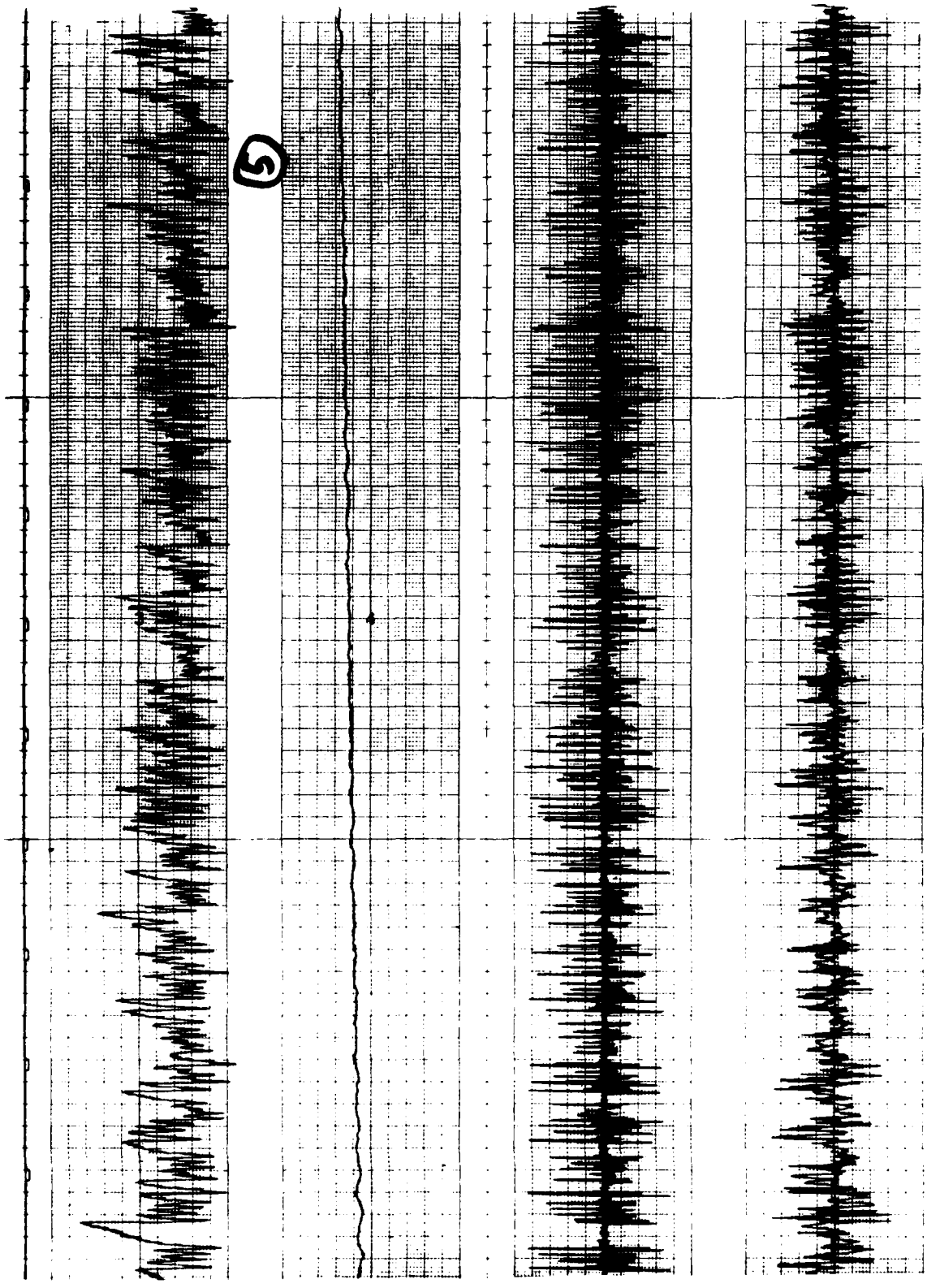
5

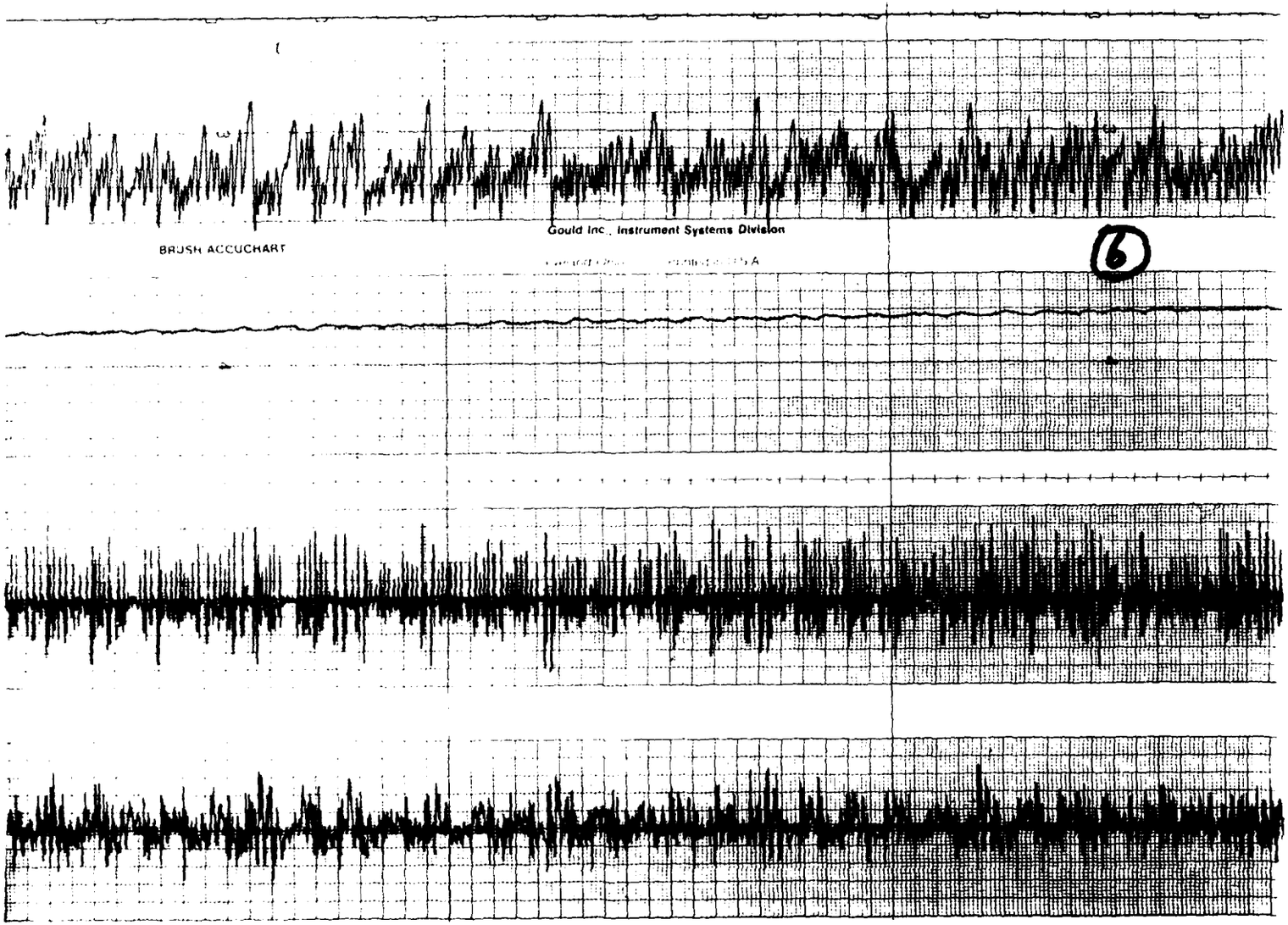
BRUSH ACCUCHART
Gould Inc., Instrument Systems Division
6

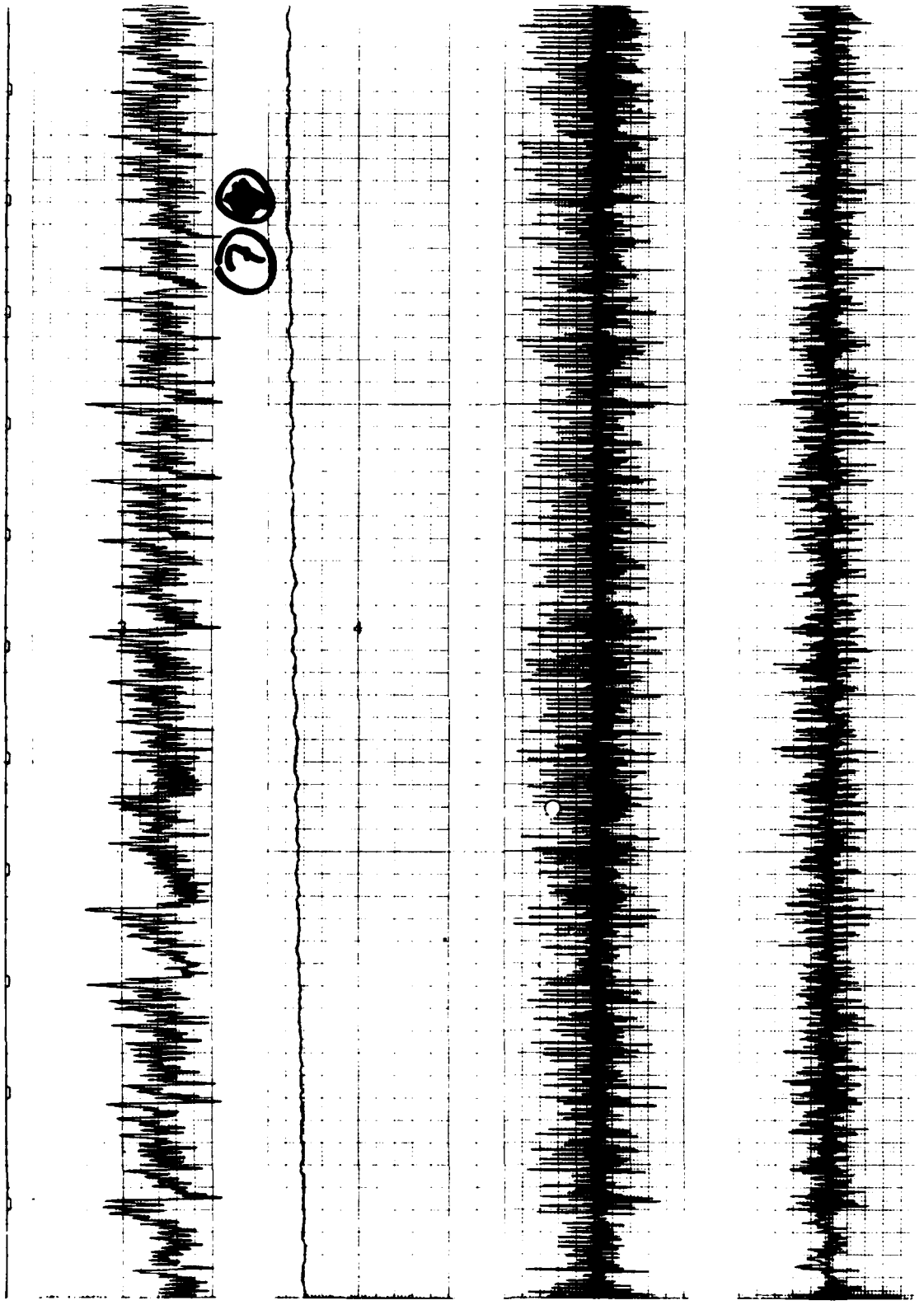

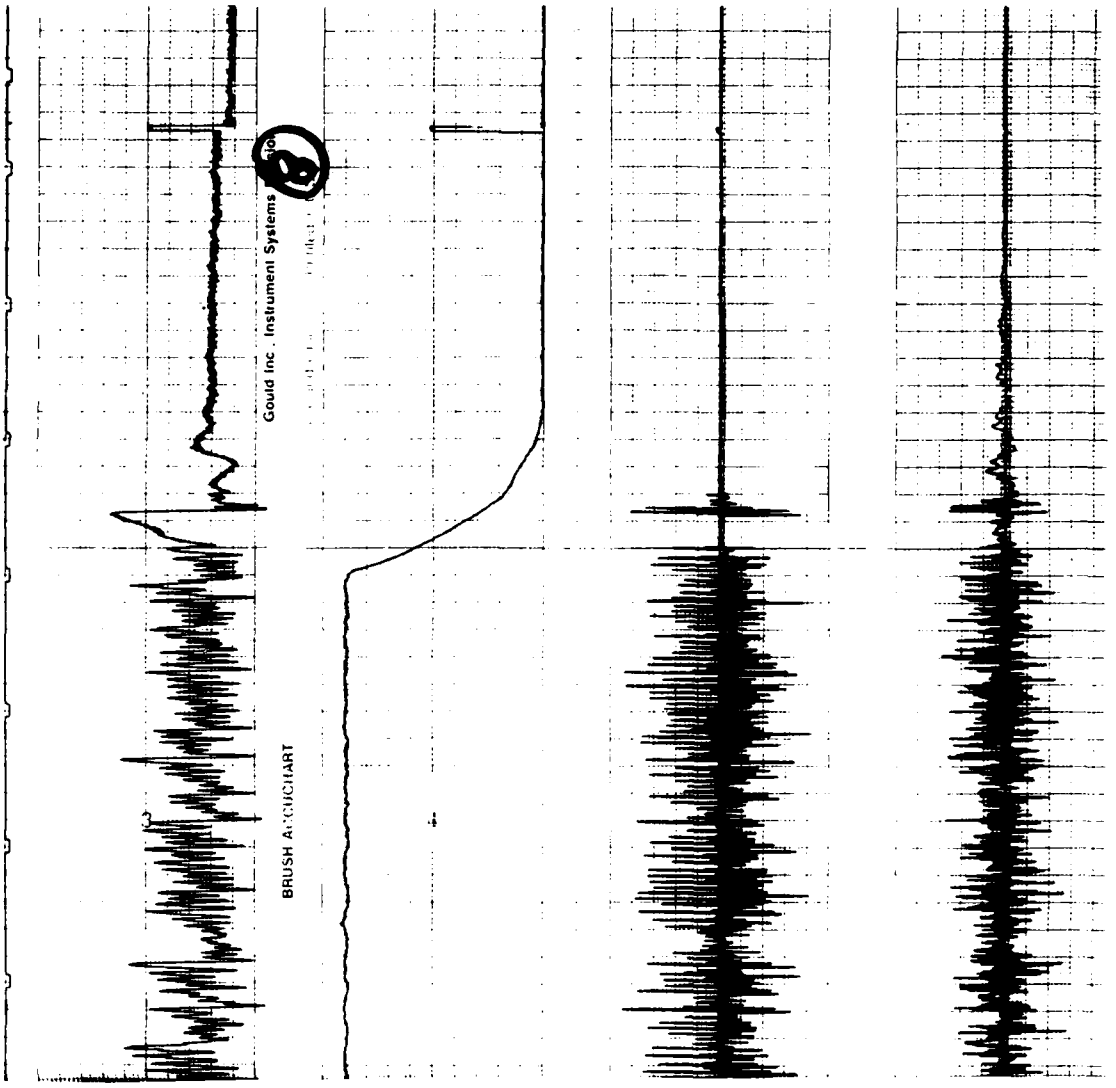
Gould Inc. Instrument Systems
BRUSH ANCHART

A facsimile catalog card in Library of Congress MARC format is reproduced below.

Määttänen, Mauri
Dynamic ice-structure interaction during continuous crushing / by Mauri Määttänen. Hanover, N.H.: U.S. Cold Regions Research and Engineering Laboratory; Springfield, Va.: available from National Technical Information Service.
iv, 53 p., illus.; 28 cm. (CRREL Report 83-5.)
Bibliography: p. 22.
1. Ice. 2. Structural properties. 3. Pile structures. I. United States. Army. Corps of Engineers. II. Cold Regions Research and Engineering Laboratory, Hanover, N.H. III. Series: CRREL Report 83-5.

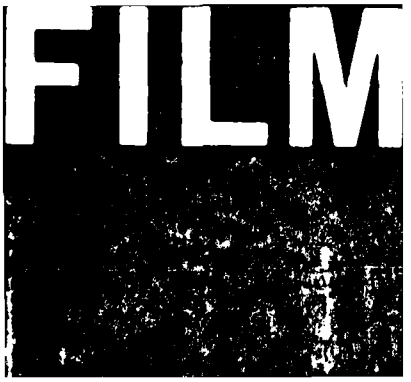
FILM